ROYAL SOCIETY
OF CHEMISTRY

Check for updates

70 years of bilirubin sensing: towards the point-of-care bilirubin monitoring in cirrhosis and hyperbilirubinemia

Jean Pierre Ndabakuranye, [iD] *[ab] Shiqiang Li, [iD][c] Genia Burchall,[d] Kate Fox, [iD][b] Terry Piva, [iD][d] Zhangyu Xu,[e] Omid Kavehei, [iD][efg] Steven Prawer [iD][a] and Arman Ahnood [iD] *[ab]

Bilirubin is clinically confirmed as a biomarker for liver health and has been utilized to implement the prognostic systems for cirrhosis and hyperbilirubinemia. Optical and chemical methods have been developed and are widely used to determine blood bilirubin levels within clinical settings. However, due to their instrument complexity, high cost, and space requirements, the existing bilirubinometric technologies do not lend themselves to point-of-care (PoC) applications within the community settings or for real-time monitoring. Consequently, bilirubin monitoring can only be monitored intermittently, resulting in missed episodes that may otherwise require clinical interventions. This review paper aims to explore potential strategies for real-world point-of-care applications. Part one discusses the metabolic pathway of bilirubin and the epidemiology of liver cirrhosis and neonatal hyperbilirubinemia. Part two provides a comprehensive review of existing bilirubinometric techniques and highlights the need for point-of-care bilirubin monitoring. Part three develops a theoretical framework for bilirubin spectroscopy. It explores two potential bilirubin measurement approaches: the multiwavelength (based on the distinct optical signatures of bilirubin) and the photodegradation kinetics approach (which relies on bilirubin degradation under blue light irradiation). Part four outlines future recommendations and provides a perspective towards three possible PoC bilirubin measurement devices for real-world applications, including a homecare testing system, a miniature implant and a neonatal wearable patch. These devices provide an opportunity for extending the reach of bilirubin measurement in locations outside hospitals and clinics.

1. Epidemiology and pathophysiology of cirrhosis and neonatal hyperbilirubinemia

1.1. What is bilirubin, and why should we care?

1.1.1. Physiological pathways of bilirubin. Bilirubin (formula: $C_{33}H_{36}N_4O_6$, molecular weight: 584.67 g mol^{-1}) is a yellow-orange by-product of haemoglobin catabolism. It is a toxic compound, so should be excreted out of the body. It

^{a} *School of Physics, University of Melbourne, Parkville, VIC 3010, Australia.*
E-mail: jeandabak72@gmail.com
^{b} *School of Engineering, RMIT University, Bundoora, VIC 3083, Australia.*
E-mail: arman.ahnood@rmit.edu.au
^{c} *Central Research Institute, 2012 Laboratories, Huawei Technologies Co. Ltd, Shenzhen, Guangdong 518129, China*
^{d} *School of Health and Biomedical Sciences, RMIT University, Bundoora, VIC 3083, Australia*
^{e} *School of Biomedical Engineering, The University of Sydney, NSW 2006, Australia*
^{f} *ARC Training Centre for Innovative BioEngineering, The University of Sydney, NSW 2006, Australia*
^{g} *Sydney Nano Institute, The University of Sydney, NSW 2006, Australia*

naturally exists as water-insoluble unconjugated bilirubin (UCB) and water-soluble conjugated bilirubin (CB). Their chemical structures are shown in Fig. 1a.

The metabolic pathway of bilirubin is schematically shown in Fig. 1b. When an erythrocyte or a red blood cell (RBC) reaches its full lifespan (usually 100–120 days), it is engulfed by a macrophage and its haemoglobin (Hb) content is released. Hb unit houses four subunits, each consisting of a protein chain (globin) and heme. At this point, Hb dissociates into heme and globin. The globin chains are broken down and are recycled as amino acids. Haem component is further degraded into iron (Fe^{2+} will later be reused in making new RBCs), carbon monoxide and UCB. It is reported that this breakdown produces between 250 and 350 mg of water-insoluble UCB in healthy adults every day.[10] The UCB then binds with albumin and is taken to the liver *via* the bloodstream. In the liver, uridine diphospho-glucuronosyltransferase (UDP-GT) enzymes attach glucuronic acid to UCB. The latter becomes the CB which is excreted in the bile and then into the intestine. At this stage, stercobilinogen is created and then oxidized to stercobilin. A different closely related secretion variant known as urobilinogen

is absorbed into the bloodstream and is sent to the kidneys. At this stage, urobilinogen is converted into urobilin *via* oxidation and ultimately excreted into urine.[12] Total serum bilirubin (TSB) levels in healthy adults range from 0.15 mg dL^{-1} to 1.2 mg dL^{-1}, of which more than 75% is UCB.[13]

1.1.2. Pathological levels of bilirubin in the blood. Bilirubin levels can fluctuate physiologically between 1.2 and 2.95 mg dL^{-1} but rarely exceed 5 mg dL^{-1}.[14] However, in the cirrhotic stage (for adults) or hyperbilirubinemia (for newborns), levels can rise to 20 mg dL^{-1},[15] and in severe cases, 50 mg dL^{-1} can be reached.[16] Elevated bilirubin levels (≥ 2.95 mg dL^{-1}) are always associated with pathological disorders, including hemolytic anemia, impaired liver function, and bile duct blockage.[17] Under such pathological states, the UCB–albumin binding capacity is exceeded. Free UCB then diffuses into the surrounding tissues leading to

observable jaundice in the skin, sclera, or mucous membrane. In extreme circumstances, UCB can accumulate in the grey matter, potentially causing kernicterus and sometimes death.[18] Therefore, accurate and timely estimation of bilirubin levels must be carried out to diagnose and forecast liver dysfunction or any underlying metabolic disorders.

To simplify the bilirubin metabolic pathways, the model in Fig. 1c is used in the form of an open-loop system. This analogy for bilirubin conversion implies that the production of UCB is independent of its conjugation and excretion. Notice that the failure of the conjugation control action is principally due to hepatocyte destruction in cirrhosis and insufficient UDP-GT enzymes production in infants. The latter can be bypassed by phototherapy, a commonly known intervention in paediatric medicine where bilirubin is decomposed into other excretable bilirubin forms *via* blue light irradiation. The following

Jean Pierre Ndabakuranye

JP received his M.S in Electronics Engineering from Hallym University (South Korea) in 2016 and is currently pursuing a PhD in Electrical and Biomedical Engineering at the University of Melbourne (Australia). His research focuses on biomedical engineering (at large), circuits and systems, semiconductor technology, optical and electrochemical sensing, photochemistry, medical microdevices, and data and energy telemetry. He has collaborated with researchers from around the world and has published multiple papers in multiple areas. He has held several sessional teaching positions at the University of Melbourne and RMIT University since 2017.

Shiqiang Li

Dr Shiqiang (Mike) Li received the B.S. degree in Materials Science from the National University of Singapore in 2007, and the Ph.D. degree from Northwestern University, Evanston, Illinois in 2014. From 2014 to 2017, he was a research fellow in the department of Electrical and Electronics Engineering at the University of Melbourne in Australia. From 2017 to 2020, he was a research scientist in A*STAR in Singapore. He is now a technical leader in Huawei Central Research Institute and specializes in Photonic theory and applications. His research interests include optoelectronic devices based on nanotechnology, meta-materials, spatial light modulators, and the multipole theory.

Genia Burchall

Dr Genia Burchall is an experienced Haematology teaching and research academic with over 15 years of experience in the higher education sector, who obtained an undergraduate & master's degree in Medical Laboratory Science and completed her PhD in 2018 also with RMIT University, Melbourne. Genia has published several articles in high impact journals in the areas of Haematology. Her interests lie in improved diagnosis and treatment of patients with a variety of erythrocyte disorders and infections of the blood, and those affecting the haemostatic system.

Kate Fox

Kate Fox is a professor of biomedical engineering at RMIT University. She has a strong interest in medical devices and materials to interact with the human body.

sections will expand on liver cirrhosis and neonatal jaundice as the primary manifestations of bilirubin.

1.2. Liver cirrhosis

1.2.1. Pathophysiology of liver failure. The liver is situated in the upper right abdominal region beneath the diaphragm and above the stomach. Its dimensions and weight can vary depending on gender, age, and body size. In adults, the liver has an average weight of about 1.5 kg and is the second-largest organ by mass behind the skin, making it the largest internal organ. The liver performs vital roles in blood detoxification, production of blood coagulation proteins, storage of minerals and vitamins, metabolism of fats, and activation of immune system to fight infectious organisms, to name a few.[19] The basic liver layout and anatomy are shown in Fig. 2a.

Hepatocyte destruction can occur when the liver is subject to pathogenic attacks (viral or bacterial) or constantly processes alcohol. However, the liver has a powerful ability to tolerate acute physical and biochemical injuries whereby hepatocytes divide and proliferate to replace the damaged and dying cells, a process known as *liver regeneration*. Conversely, when the liver is subjected to chronic injuries, it can be scarred to the point where

Terry Piva

Terry Piva is an Associate Professor at RMIT University. He is a biochemist/cell biologist by training having completed his PhD in tumour metabolism. He currently teaches biochemistry, immunology as well as tumour and cell biology to undergraduate and postgraduate students, as well as supervising a number of PhD projects. His research is focused in melanoma signaling pathways, but he retains an interest in cellular metabolism, and brings his expertise in understanding the formation and excretion of bilirubin and of diseases where these processes are affected in individuals.

Omid Kavehei

Dr Kavehei is an academic and research leader at The University of Sydney. Before this appointment, he was with the Centre for Neural Engineering at The University of Melbourne. He was awarded his PhD in Nanoelectronics from the University of Adelaide in 2012 with the Postgraduate University Alumni Medal and the 2011 South Australian Young Nanotechnology Ambassador award. In 2014, he was a Visiting Project Scientist at the University of California, Santa Barbara. In 2021 he was part of a team who won the Ramaciotti Awards for Biomedical Research. He is a Senior Member of IEEE.

Steven Prawer

Steven Prawer is Professor of Physics at the University of Melbourne. He has a worldwide reputation in advanced diamond science and technology with over 35 years of experience and over 420 scientific publications. His research initiatives are dedicated to using science, engineering, and technology to address problems of global significance. He has, among other things, been a senior leader for one of Australia's most prestigious projects namely the development of a bionic eye and has developed the technology for the fabrication of diamond-based quantum devices, such as single photon sources for secure communications, and bionic devices for retinal stimulation and neural recording for forecasting epileptic seizures. He has cofounded 3 start-ups; quantum communications Victoria, iBIONICS, and carbon cybernetics. He was elected to the Australian Academy of Science in 2010 in recognition of his contribution to diamond science and technology.

Arman Ahnood

Dr Arman Ahnood received M. Eng in engineering from University of Cambridge in 2006 and Ph.D. in electronics and electrical engineering from University College London in 2011. He is currently a lecturer at the School of Engineering, RMIT University. His research focuses on using consumer electronics advances to address biomedical challenges. He has held various positions with Philips Research Lab, Universities of Cambridge, and Melbourne. He has authored over 60 papers in the fields of bionics, as well as electronic materials, devices, and systems. In the past five years, he has co-founded two companies, Carbon Cybernetics Pty. Ltd. and BrainConnect Pty. Ltd.
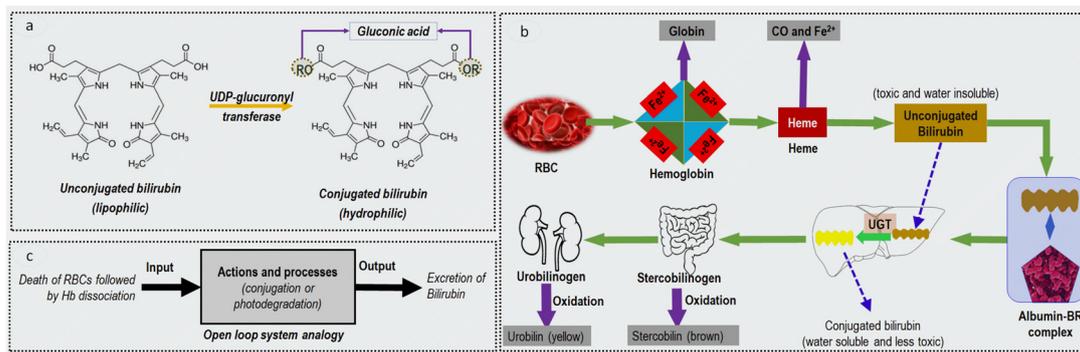
Fig. 1 (a) Bilirubin chemical structure. The left shows the unconjugated or indirect bilirubin, whereas the right shows the conjugated or direct bilirubin. The two forms of bilirubin differ from each other with the attached radical after conjugation. (b) Bilirubin pathway: Hb (released from senescent or damaged RBC) breaks down into globin and heme. Heme is then degraded into unconjugated bilirubin (water-insoluble); the latter binds with albumin and is taken to the liver. In the liver, the enzymes act upon UCB to become conjugated bilirubin (water-soluble) which is excreted from the body *via* stool and urine. (c) An open-loop system analogy of bilirubin excretion. The actions include all the steps involved from the albumin binding to the bilirubin conjugation or the photochemical degradation of bilirubin during phototherapy.

the damage may become irreversible. This late stage is called *cirrhosis* and is characterized by a histological formation of regenerative nodules surrounded by fibrous bands (Fig. 2b) and an ultimate disruption of the hepatic architecture.[20]

Cirrhosis has two major stages: compensated cirrhosis and decompensated cirrhosis. Compensated cirrhosis is when the liver is moderately damaged (usually before any major complication is developed) and can still perform essential functions. In contrast, decompensated cirrhosis is
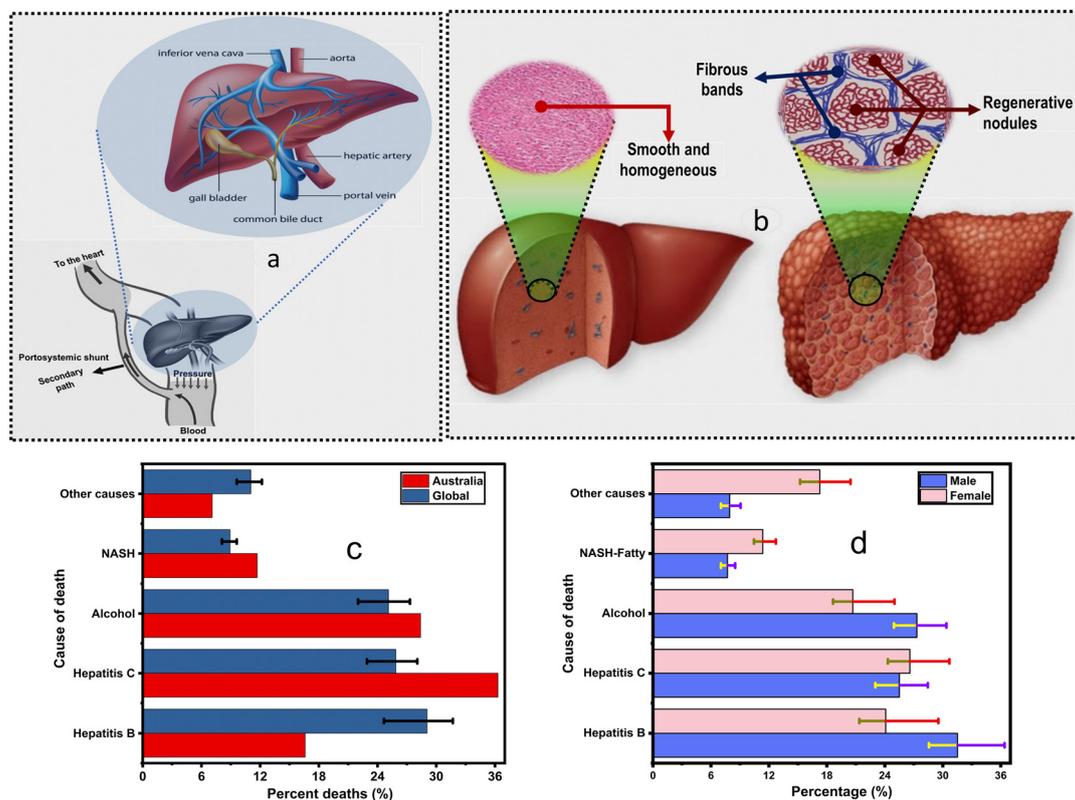

Fig. 2 (a) Basic anatomy of the liver. It consists of a hepatic artery and portal vein; these combine to form a sinusoid that prolongs into the central vein and is aligned with hepatocytes and the bile duct.[2] Various important parts of the liver are labelled. (b) Liver layout: healthy liver (left) *vs.* cirrhotic liver (right). The inset shows the histology of cirrhotic tissue with regenerative nodules formed when liver cells are injured. These nodules can be thought of as colonies of hepatocytes. In between the nodules, there are fibrous bands. This figure is used with permission from Mayo Clinic. (c) Global distribution by causes of death by gender. (d) The distribution of death by liver failure causes; hepatitis C and hepatitis B are the most common causes in Australia and globally. Other causes include drug-induced injuries and hemochromatosis.[6]

characterized by various severe pathologies and is the primary cause of death in end-stage liver disease.[21] At this stage, the liver fails to accommodate some of its physiological functions, such as blood detoxification and filtering. Thus, toxins, such as bilirubin, will be dumped into the central circulatory system without being filtered out, leading to elevated levels in the blood (Fig. 2a). By monitoring their blood levels, toxins can be used as biomarkers for physiological and pathological processes in the liver, and indeed, this is the primary motivation of this review.

1.2.2. The burden of cirrhosis: statistics and healthcare costs. Cirrhosis is an epidemiological concern and a major source of morbidity and mortality (Fig. 2c and d). It results in ~1.5 million annual deaths accounting for 3.5% of global deaths. It is also the eleventh most common cause of death globally and the third in people aged between 45 and 65.[22,23] Liver diseases consume substantial economic resources from individuals and governments, emanating from direct costs (drugs, hospitalization, transplantation, government funding and more) and indirect costs (reduced work productivity and failure to re-join the workforce).[6] Some of the therapeutic procedures such as palliative care, extracorporeal liver support, and liver transplantation are the major contributors to the financial costs. The cost of liver diseases in the Commonwealth of Australia was estimated at ~AU$ 51 billion in 2012, including direct financial costs and the burden of disease.[24] In 2022, the mentioned cost is likely to be higher than a decade ago.

1.2.3. Clinical course: diagnosis, prognosis, survival, and death. Despite its frequent presentation, cirrhosis can be challenging to diagnose and, once established, difficult to treat.[25] Diagnostic procedures may include blood tests, liver biopsy and imaging techniques (ultrasonography, computed tomography scanning and Magnetic Resonance Spectroscopy).[26] Studies have attempted to predict the prognosis of cirrhosis using Model for End stage Liver Disease (MELD) and Child-Turcotte-Pugh (CTP) scores. However, although these scores are clinically used in predicting short term and long term survival, their prognostic significance presents complexity, i.e., they require multiple input variables.[27]

It is, however, essential to recognize that there is a certain degree of survival in patients with cirrhosis. For example, Sumskiene et al.[28] reported a mortality rate of 51.1% in 17.9 months and D'Amico et al.[29] reported an average survival rate of 50% in 24 months. In these studies, higher survival rates were observed in patients with low TSB levels. In general, the degree of hepatic dysfunction is a critical determinant of both prognosis and therapeutic interventions.

One of the liver's primary functions is to conjugate and excrete bilirubin; therefore, liver failure causes blood bilirubin levels to rise. Lopez-Velazquez et al.[30] determined bilirubin as the sole biomarker for predicting mortality in cirrhotic patients. They compared the prognostic effect of bilirubin to MELD and CTP scores and showed that bilirubin was as a significant mortality determinant. The area under curve and p-values of are CB = 0.751 (p = 0.001), UCB = 0.724 (p = 0.002), TSB = 0.746 (p = 0.001), MELD = 0.653 (p = 0.037), and CTP = 0.684 (p = 0.012).[30] Other studies have been carried out and supported the findings of Lopez-Velazquez et al. that bilirubin is a biochemical indicator of liver health.[31,32]

1.3. Neonatal jaundice and bilirubin photodegradation

1.3.1. Pathophysiology of neonatal jaundice. Jaundice (the skin's yellowing) is one of the prevalent conditions in infants and requires medical attention from the outset. Virtually all infants will incur bilirubin levels above the healthy upper limit (1.2 mg dL^{-1}).[12] However, a slightly increased bilirubin does not need to be tested or treated. It is reported that more than 60% of all full-term health newborns and 80% of all preterm newborns will incur jaundice in the first week after birth.[33] This occurs as the infant transitions from relying on the placenta to the complete dependence on the hepatobiliary system for bilirubin excretion.

There are three main causes of elevated bilirubin levels in this age group: (1) infants typically have a high haematocrit count (over 60%).[34] Some foetal RBCs are relatively unstable and will quickly break down, increasing the produced amounts of UCB. (2) The neonatal hepatic system is not sufficiently developed to regulate and mobilize enough UDP-GT conjugation enzymes, leading to the inefficient removal of bilirubin. (3) The intestinal system has not sufficiently developed a stooling pattern; this slows the digestion process and increases the enterohepatic reuptake of the bilirubin leading to an imbalance between bilirubin conjugation and excretion. The mentioned three factors will inevitably lead to a diminished clearing ability and an ultimate increase in bilirubin levels.

Although the neonatal development of mild jaundice physiological, these factors are expected to go away in a few days. Levels will usually peak at ca. five days, and jaundice will resolve at a 1 week margin. During this period, bilirubin levels will more often than not stay below 12 mg dL^{-1}.[35] Conversely, pathological jaundice may also occur, and although less common, it still affects about 5% of infants.[36] It involves a TSB measurement higher than the threshold, however, this will vary based on the gestational age and birth weight of the infant.[37] The comparison between physiological jaundice and pathological jaundice is given in Table 1.

Hyperbilirubinemia is a sign of bilirubin levels above 1.2 mg dL^{-1}, which is the upper limit in healthy adults.[38] Depending on the dominant variant, hyperbilirubinemia can be categorized as unconjugated (indirect) or conjugated (direct), but the former is the most common. Severe hyperbilirubinemia may, in some instances, imply that the infant has other contributing factors such as the exposition to an infection or the existence of genetic or metabolic conditions.

Hyperbilirubinemia can be thought of as a spectrum. Simple physiological jaundice manifests at low levels, and

Table 1 Summarized comparison between the characteristics and criteria of physiological jaundice and hyperbilirubinemia

Criteria	Physiological jaundice	Pathological jaundice
Visible in the first 24 hours after birth (first day of life)	No	Maybe
Variation in total serum bilirubin levels	Up to 5 mg dL^{-1} each day for a maximum of five days	More than 5 mg dL^{-1} each day
Variation in conjugated bilirubin levels	Maximum of 2 mg dL^{-1} or 20% of the total serum bilirubin	More than 2 mg dL^{-1} or 20% of the total serum bilirubin
When is jaundice expected to end?	In seven days (one week) for full-term neonates and two weeks for premature neonates (<37 weeks gestational period)	May take longer

mild jaundice may exist without an underlying cause. As bilirubin continues to increase, the infant may start to encounter increased sleepiness, and at the level of 17 mg dL^{-1}, phototherapy can be recommended.[39] Rarely the TSB levels above 25 mg dL^{-1} are reached.[40] At these bilirubin levels, the neonates will be at risk of developing a condition known as *bilirubin-induced neurologic dysfunction* (BIND). At this stage, bilirubin may cross the blood–brain barrier to bind with the brain tissue, especially the basal ganglia.[40] The most important interventions to reduce TSB levels in infants are enteral feeds, phototherapy, and blood transfusion.[40] Herein, we focus on phototherapy.

1.3.2. Phototherapy as a treatment of neonatal jaundice. Phototherapy refers to a treatment that uses light to improve a medical condition by alleviating or hindering its development. It mainly uses visible light from artificial sources, excluding therapies that require high optical power or photosensitizing agents such as tissue sterilization or photochemotherapy.[41]

It has been reported that sunbaths were used as a form of phototherapy in ancient Egypt, China, Roma, and Greece to maintain general health.[41] The early and distinguished work for clinical phototherapy was done by Niels Finsen, in which red light was used to impede scarring and inflammation in patients with smallpox.[42] He further designed a device with quartz lenses and filters to treat lupus vulgaris, a form of cutaneous tuberculosis.[42] The technology was gradually improved over the years and was utilized to treat pulmonary tuberculosis, rickets and various diseases.[42,43]

Perhaps the most critical and unique success story is the utilization of phototherapy to treat neonatal jaundice, which is presently established and applied in paediatric care as a safe and easy to use technique.[44] It was first introduced in 1958 by Perryman *et al.*[44] from the General Hospital of Rochford, Essex. However, it was not widely adopted and coined until proven safe and effective, a decade later.[45]

1.3.3. Mechanisms of blue light phototherapy. Although discovered solely based on an accidental observation with no scientific principles,[44,46] it is currently known that blue irradiation induces photochemical reactions that alter the structure of bilirubin without any changes in its constitution (same empirical formula but different structural arrangements). When bilirubin in the skin absorbs light, the chemical reaction is initiated where bilirubin is converted into byproducts that can bypass the liver's conjugation

mechanisms and be eliminated from the body *via* the intestinal or urinary tracks. Moreover, the byproducts are less likely to permeate through the blood–brain barrier, which could otherwise increase the risks of neurological damage. Phototherapy will clinically be recommended to prevent the elevation of bilirubin to TSB above 20 mg dL^{-1} or blunt the rising rate of TSB.[40]

Bilirubin phototherapy usually requires a blue optical source, and various reports suggest that the range of 430 nm to 490 nm is more efficient and effective than other visible ranges.[47] The three most common pathways of bilirubin photodegradation include photooxidation, structural isomerization, and configurational isomerization. It is claimed that lumirubin is the primary pathway by which phototherapy gets rid of bilirubin from the body.[40]

1.3.4. Prevalence and economic burden of neonatal hyperbilirubinemia. The national and global prevalence of neonatal hyperbilirubinemia is less known due to the absence of large-scale studies documenting these incidences.[48] Besides, there is no definite cutoff above which the incidence can be labelled as hyperbilirubinemia.[49] Maisels suggested that it can be labelled as so if the bilirubin levels are above the 95th percentile for a given population.[50] However, the data is unavailable for many communities and regions, making the global standard invalid.

The economic burden associated with neonatal hyperbilirubinemia is also poorly understood.[48] However, one thing is obvious: neonates are a high-risk population, and hyperbilirubinemia puts substantial financial pressure on public healthcare system resources and various associated costs on the caregivers. Thus, effective treatments and new management protocols (including testing systems) may help mitigate the overall burden of neonatal hyperbilirubinemia.

2. Current bilirubinometric techniques and limitations

Several techniques have been developed to estimate bilirubin levels, where direct spectroscopy and diazo reaction are the most prevalent in clinical use. Measurements are performed for every age group but prevalently in neonates and cirrhotic patients. Depending on the signal detected, these techniques can be classified into three groups: optical, electrical, and chemical or a combination of these. These techniques present, however, several limitations, including instrument

bulkiness and managerial proficiency requirements. The following sections will review several existing bilirubinometric techniques, including chemical, spectrophotometric, electrochemical methods and more. Various associated limitations are also discussed. Table 2 compares and contrasts between major clinical bilirubinometric methods.

2.1. Spectroscopic techniques

Spectroscopic methods are used to measure the concentration of bilirubin by applying Beer's law (equation), which describes the ability of light attenuation and absorption by a material at specific wavelengths.[51]

2.1.1. Transcutaneous technique. This technique uses reflectance measurement at two or more wavelengths to obtain BR levels (Fig. 3a and b).[52] Although this technique is comparatively low cost and user friendly, it suffers from inaccuracy. It has, however, been proven successful only in neonates since the skin of adults is thicker, and the levels of melanin and fatty cells are higher, resulting in increased spectral interferences.[41] Also, blood is localized in the vascular plexus but not uniformly distributed in the skin,[42] and skin blanching, a standard prerequisite for transcutaneous measurement,[43] may occasionally damage the users' skin.

2.1.2. Gas analyzer: photometric technique. This technique computes the total bilirubin concentration in whole blood or plasma. The blood drawn from the patient is measured at multiple wavelengths, and a computer-based algorithm is used to correlate the measurement with bilirubin concentration.[53] However, this technique requires bulky and complex equipment and specialized operators.

2.1.3. Direct spectrophotometry. Direct spectrophotometry mainly uses UV-vis full-range scanning spectrometers, and in some instances, reagents such as caffeine are required.[54] Spectrophotometric estimation of bilirubin in serum[55] and urine[56] samples has been reported. The determination of bilirubin levels by derivative spectrophotometry has also been reported.[57] Although direct spectrophotometry is accurate and reliable compared to other routine techniques, it suffers from interference with other proteins and different pigments, such as carotenoids which absorb at ~450 nm and are prevalent in infants below three weeks old.[58] Besides, it requires pre-processing of samples and reagents, bulky and
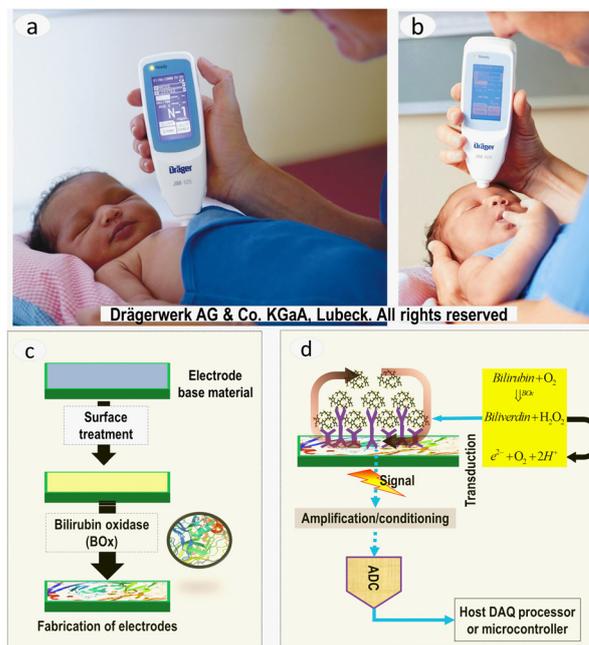
Fig. 3 (a and b) The images show newborns being measured for BR levels on the forehead (left) and sternum (right). Light is illuminated on the skin, and the reflectance is measured. The obtained information is processed and correlated with BR levels. Images were used with permission from Drägerwerk AG & Co. (c) Schematics illustrating the processes involved in fabricating and preparing bilirubin biosensors. (d) Schematic representation of chemical reactions and measurements of electrochemical response. The sensor surface with immobilized enzymes acts as an electrochemical transducer. The response measurement is achieved using an ADC for digitization and a host microcontroller/processor for data processing and acquisition.

expensive instruments, and trained staff to carry out the analysis.

2.2. Chemical techniques

2.2.1. Calorimetric assay kits. Several colourimetric assay kits exist, including Sigma Aldrich MAK126, Biovision K553100, and Cell Biolabs MET5010. These assays use the Jendrassik–Grof principle to measure the concentration of bilirubin via a reaction with a diazo salt to form azobilirubin, which absorbs at a specific wavelength; usually 550 or 600 nm. A catalyst is required for total bilirubin determination but not for conjugated bilirubin. These assay kits are,

Table 2 Comparison of the gold-standard clinical bilirubinometric techniques

	Chemical	Photometric	Transcutaneous
Accessibility	Requires outpatient visit	Requires outpatient visit	Only for full-term infants
Example of clinical models	Dimension RxL (Dade Behring),	Roche OMNI S (Roche Diagnostics)	Dräger JM-103 (Dräger Medical Inc.)
Sample type	Plasma or whole blood	Whole blood	Not applied
Cost	High-end	High-end	Comparatively low
Technical knowledge	Requires a trained operator	Requires a trained operator	Little to no training is required
Cut-off sensitivity of 100%	Not applied	~13.7 mg dL^{-1}	~12.8 mg dL^{-1}
Positive predictive value, %	Highest	High (80–90%)	Low (<50%)

© 2022 The Author(s). Published by the Royal Society of Chemistry

however, expensive and less selective. Besides, the accuracy in the diazo-based techniques is challenging since the reaction rates are pH-dependent. These kits also require both extended test preparation time and a trained staff to carry out the analysis.

2.2.2. Chemical analyzers. In this approach, blood or plasma is mixed with a reagent, and the amounts of formed colloidal BR complexes are measured. Although chemical techniques have shown high accuracy, devices are bulky and complex and require experienced and specialized operators. They also involve clinical procedures; patients must attend the hospital where blood is drawn (usually by venipuncture) and measured for BR. Turn-around-time can be lengthy, resulting in delayed diagnosis and poor prognosis. Besides, patients may miss scheduled appointments due to disability, substance abuse, and existing medical conditions.

2.2.3. Paper-based techniques. In addition to aforementioned chemical methods, paper-based colorimetric assays have also been attempted and developed for bilirubin measurements.[59,60]

2.3. Chromatographic techniques

2.3.1. Thin layer chromatography. Thin Layer Chromatography (TLC) involves separating non-volatile mixtures on glass, aluminium, or plastic adsorbent substrate (*stationary phase*), usually coated with silica gel. *Via* the capillary action, the mixture (*mobile phase*) is pushed upwards, leading to the separation of substances due to the difference in ascending rates or concentrations. In 1984, Shinya analyzed the azo-pigments derived from bilirubin tetrapyrroles in bile using the TLC technique.[61] Although experimentally easy and economical, TLC is susceptible to moisture and temperature.

2.3.2. High-performance liquid chromatography. In analytical chemistry, the High-Performance Liquid Chromatography (HPLC) process starts with separating a solvent mixture into individual components, followed by identifying and quantifying these components. A pump is required to maintain a constant flow through the column, at which point a detector gives a retention time characteristic of the analyte of interest. Spivak and Yuey developed an efficient reverse-phase HPLC technique to estimate bilirubin which was further used to diagnose biliary tract hindrance and Crigler Najjar condition.[62] Other studies for bilirubin determination using HPLC have been reported.[63–67] Although HPLC exhibits high resolution, reproducibility, and precision, it is time-consuming and requires costly reagents, bulky equipment and managerial proficiency.

2.4. Capillary electrophoresis

Capillary electrophoresis (CE) involves separating an array of tiny molecules using narrow capillary tubes or micro/nano-fluidic channels. CE has primarily been used in evaluating free and bound bilirubin. CE has also been coupled with frontal analysis (FA) to monitor the evolution of free bilirubin in infants, thus revealing the information about bilirubin–albumin binding affinity.[68,69] A CE-based microfluidic microsystem has also been reported for bedside monitoring.[70,71] Although CE is a low cost, quick, and reproducible technique, it requires expertise for handling.

2.5. Electrochemical bilirubin biosensors

Electrochemical sensors are a class of sensors that incorporate a biological (or a biologically derived) material with a transducing microsystem. The reaction with the analyte of interest gives rise to a signal as an electrochemical response. Depending on the measured property (current, potential and impedance), electrochemical sensors can be categorized into three groups: amperometric, potentiometric and impedimetric biosensors.[72]

Electrochemical biosensors first appeared during the second half of the 20th century with the first reported oxygen electrode[73] and the invention of glucose sensors, as proposed by Clark and Lyons.[74] Currently, most commercial biosensors are targeted for clinical applications such as testing glucose, urea, creatinine, cholesterol, and lactate.[75,76]

Bilirubin electrochemical biosensors are generally based on catalytic oxidation of bilirubin into biliverdin. The oxidation catalyst is known as *bilirubin oxidase* (*BOx*). The major steps involved in fabricating bilirubin biosensors and measuring electrochemical response are shown in Fig. 3c and d. In 1989, Moussa *et al.* first reported the electrochemical oxidation of bilirubin in dimethyl sulfoxide;[77] and since then, various studies on electrochemical sensing of bilirubin have been reported. Various bilirubin biosensors that use precursor materials have been reported. They include dissolved-oxygen,[78] conducting polymer,[79] nanoparticles,[80] and sol–gel.[81] Bilirubin estimation by coupling with other sensing capabilities, including photo-electrochemical,[82] piezo-electrochemical sensors,[83] opto-electrochemical,[84] electro-chemiluminescent[85] sensing has also been reported. These biosensors are notable because they (1) generate no waste and thus are considered clean, (2) can be miniaturized into portable devices that require micro-volume samples, and (3) are highly selective and cheap, allowing their popularization.[72]

2.6. Fluorometry

Fluorimetry involves measuring the spectral emission intensity and distribution of a specific optical spectrum after excitation. Fluorometry has been applied to quantify bilirubin by reacting a fluorescent derivative with BOx and measuring the emission at 440 nm after a 240 nm excitation.[86,87] Brown *et al.* developed a fluorometric method and used it to measure UCB and TB concentration and estimate bilirubin-albumin binding capability in blood specimens from 79 neonates.[88] Several other fluorometric studies on bilirubin estimation have been reported.[86,89] Although remarkably sensitive and portable, fluorometry is prone to inaccuracy

due to variations in pH and temperature and requires costly instruments and complex measurements.

2.7. Chemiluminescence

Chemiluminescence (CL) involves light emission after a chemical change with no heat production. Recent attention has been received to measure bilirubin using a conjunction of chemiluminescence and flow injection analysis (FIA). By inhibiting the CL from the lucigenin – hydrogen peroxide (H_2O_2) complex, the negative correlation between the CL intensity and bilirubin concentration can be used to measure bilirubin levels in humans.[90] Huie *et al.* detected a CL emission from bilirubin in natural solvents due to its reaction with peroxyoxalate; however, the limitations emanate from the solubility of CL reagents, and the quenching of CL intensity in aqueous media are critical.[91] Calokerinos *et al.* updated the technique and measured bilirubin in the presence of water and various oxidizing agents.[92,93] Several other studies were also reported.[94,95]

2.8. Polarography

Polarography is a particular kind of linear sweep voltammetric technique in which the electrode potential is adjusted linearly. The use of differential pulse polarography to estimate bilirubin and its derivative at a mercury electrode has been reported.[96] Several other studies on bilirubin estimation by polarography have been reported.[97,98] Although polarography has higher sensitivity and a lower detection limit, it is prone to stray voltages from wires and nearby sources.

2.9. The need for point-of-care bilirubin estimation

During the post-industrial revolution era, science and engineering have forever transformed the world's political and socioeconomic landscapes. They have significantly morphed and influenced nearly every facet of modern society and eventually allowed healthier, longer and more stable lives. Humankind can now witness the impacts of this incredible technological journey and, at the same time, foresee vast, exciting future developments that can meet new and future challenges.

The past few decades have seen an evolution of various medical technologies that have transformed healthcare. These breakthroughs were made possible by humankind's ability to master the micro-and nanoscale, which led to the miniaturization of devices. These breakthroughs have been motivated by a remarkable increase in socio-political awareness for monitoring many biomedical practices ranging from minor to deadly diseases to improve human health. The latter is due to the ceaseless recognition of new conditions, bringing new engineering and clinical sciences challenges to develop innovative and optimal techniques for POCT, diagnosis, and treatment of diseases. These techniques must be tailored for real-time and continuous detection of diseases, either *in vitro* or *in vivo*, while delivering fast and

Table 3 Advances in the development of point-of-care

Technology reference	Method	Estimated cost [AU$]
Yamanouchi, *et al.*[52]	Handheld	—
Jacques, *et al.*[99]	FOC-based	—
SpectRx BiliCheck[100]	Handheld	2300
Bilistick[101]	Fingerprick	1400
JM-103 (ref. 102)	Handheld	1500
JM-105 (ref. 102)	Handheld	2900
KJ-8000 meter103	Handheld	4800

accurate results. Thus, there is no doubt that research into the effective techniques for bilirubin levels estimation will continue to grow.

The real-time bilirubin levels measurement is essential in tracking liver health. The information on its temporal distribution is often entailed to accelerate decision-making in homes or hospitals (*i.e.*, in emergency room and intensive care units). Fast and self-administered POC devices can reduce the frequency of unnecessary and missed clinical visits and make patients much more responsible for their conditions (some of the devices on the market are shown in Table 3). Moreover, miniaturization is currently essential in sensor technology to achieve simple, low cost and portable devices usable in remote areas for emergency purposes thus, shifting from clinical settings into non-laboratory settings. Considering the limitations of the current bilirubinometric techniques, the substantial socioeconomic impact associated with cirrhosis, and recent findings identifying bilirubin as a sole biomarker of liver health, an effective point-of-care bilirubin sensor that supplements outpatient visits would be useful. These POCT techniques include implantable, wearable, and handheld devices and sensors.

3. Bilirubin spectroscopy

3.1. An overview of optical methods in biochemistry

Optical methods are based on how a substance interacts with electromagnetic radiation, usually referred to as light in spectroscopy. The light-matter interaction exhibits typical optical properties, including absorption, emission, refraction or bending, reflection, scattering, or delayed emission. These properties can be measured and correlated with the amount of a substance.[104] Through direct or indirect measurements, the optical properties can be quantified and be used to identify the physiological and pathological processes in the body.

Direct optical techniques, such as diffuse reflectance measurements, have been used to measure blood flow, heart rates, and oxygen saturation.[105] Perhaps the most widespread application of the direct optical method is pulse oximetry. On the other hand, indirect optical techniques involve chemical reactions of the analyte with precursor reagents to form an optically measurable product. For example, in the Jendrassik–Grof method, bilirubin reacts with a diazotized

sulfanilic acid to produce an azo dye that is optically measurable at 550 nm and proportional to bilirubin concentration.[106,107]

Among other optical methods, spectrophotometry is perhaps the most thought-after quantitative analytical chemistry technique with applications in life science and clinical settings. Whilst full-range spectrophotometry can be used in laboratory settings to determine accurate and reliable results, in some instances, it is impractical owing to instrument complexity, bulkiness (weight and size) and susceptibility to mechanical shocks. Cadusch *et al.* have attempted to develop a lightweight visible range spectrometer.[108] Although this is a comparatively convenient solution, the complexity and cost are still high.[108] Hence, an optimal selection of a smaller number of wavelengths for this purpose could enable mobile medical devices with significantly lower power consumption at an exponentially lower cost. However, this can be at the expense of lower measurement accuracy. The error increases with the reduction in the number of selected wavelengths, and the error analysis for the measurement will be discussed later. At a minimum, the absorption measurement at two wavelengths is necessary to perform a quantitative analysis of blood composition. This approach is commonly referred to as dual-wavelength measurement. Indeed, this same approach is selected in most commercial pulse oximeters.

The viability of optical measurement in blood relies on the validity of three key requirements. The first requirement is essential for *in vivo* measurements, whilst the remaining two apply to both *in vivo* and *in vitro* measurements. The first requirement (*in vivo*) entails that the presence of arterial pulse is required to decouple the absorption of the tissue with that of blood. However, for *in vitro*, the arterial pulse is not present, and the setup does not need to be optimized to mitigate its contribution to the optical absorption.[109] The second requirement (both *in vitro* and *in vivo*) is that the analyte of interest should have a distinguishable optical absorption feature independent of the rest of the blood pigments. This feature is manifested in blood oximetry, where the HbO and HbR exhibit a significant difference in extinction coefficients at 660 and 940 nm wavelengths.[110] Although many other blood pigments, including other forms of hemoglobin, contribute to the optical absorption, HbO and HbR exhibit distinct spectral signatures. Thus, the interference due to these pigments can be mitigated, leading to improved accuracy in the blood oxygen content determination. It can be noted that many other blood components, such as glucose and creatinine, do not exhibit distinct spectral features in the visible range; thus, conventional optical absorption is not valid.[111] In these cases, measurements such as reagent-based indirect optical methods can be used. The third requirement is predicated upon the predictable relationship between optical absorption and concentration. In the simplest form, the optical absorption of a blood pigment would follow a linear trend with its concentration. This is famously referred to as Beer's

law, and its expression is given in eqn (1). However, several non-idealities would contribute to deviation from this relation. For example, blood exhibits a strong scattering, which could invalidate Beer's law in some instances.[112] Similarly, nonlinear absorption at higher and lower light intensities, as well as autofluorescence from a multitude of blood compounds when exposed to shorter wavelengths, are factors that can lead to deviation from the conventional Beer's law. Therefore, devices such as oximeters are designed to operate within a measurement regime in which Beer's law is a valid approximation.[113]

3.2. Beer's law and the principle of dual wavelength

3.2.1. The foundations of Beer's law and dual wavelength. Formally, the concentration C [M] of a substance in a solution relates to its absorbance A and light path length t [cm], as shown in eqn (1). This expression is widely known as Beer's law, where the molar extinction ε (λ) [M^{-1} cm^{-1}] is a constant of proportionality (T: transmittance, I_0: incident light, I: transmitted light).[51] It should be noted that Beer's law is insufficient in circumstances with significant reflectance, scattering and autofluorescence; however, within a specific range of concentrations, it has been and can be used as an approximation.[114] It is important to note that the portion of the intensity absorbed by a substance in a solution at a specific wavelength is a constant value characteristic of the material. This constant value is known as the "***absorptivity ε***" and can be related to the absorbance, as shown in eqn (1).

$$A = \varepsilon \times t \times C = -\log_{10}^{(T)}\Big|\Big|_{T=\frac{I}{I_0}} \tag{1}$$

Another essential parameter is the "***absorption coefficient***, μ_a***", which determines how deep light of a particular wavelength can go into the sample before being completely absorbed. Thus, if the material with a low absorption coefficient at a specific wavelength is thin enough, it will appear transparent. The expression of the absorption coefficient is shown in eqn (2).

$$\mu_a = \varepsilon \times C \times \ln 10 \ [cm^{-1}]\big|\big|_{I=I_{0e-\mu a \times t}} \tag{2}$$

Whilst the one-dimensional Beer's law provides an opportunity to measure the concentration of a substance in the solution at a specific wavelength, this approach is insufficient in cases where two or more substances contribute to the optical absorption of the solution. This scenario could be addressed by considering the absorption at two or more wavelengths using *n*-dimensional Beer's law approach. The two-dimensional Beer's law referred to as dual-wavelength measurement is presented in eqn (3). $\varepsilon_{x,1}$ and $\varepsilon_{y,1}$ are the molar extinction coefficients for components x and y at λ_1. $\varepsilon_{x,2}$ and $\varepsilon_{y,2}$ are the molar extinction coefficients for x and y at λ_2. C_x and C_y are the molar concentrations for components x and y. λ_1 and λ_2 are commonly referred to as analytical wavelength and reference wavelength, respectively.

$$\begin{bmatrix} \varepsilon_{x,\lambda_1} & \varepsilon_{y,\lambda_1} \\ \varepsilon_{x,\lambda_2} & \varepsilon_{y,\lambda_2} \end{bmatrix} \begin{pmatrix} C_x \\ C_y \end{pmatrix} \times t = \begin{pmatrix} A_{\lambda_1} \\ A_{\lambda_2} \end{pmatrix} \Rightarrow \begin{cases} A_{\lambda_1} = (\varepsilon_{x,1} \times C_x \times t) + (\varepsilon_{y,1} \times C_y \times t) \\ A_{\lambda_2} = (\varepsilon_{x,2} \times C_x \times t) + (\varepsilon_{y,2} \times C_y \times t) \end{cases} \tag{3}$$

Dual-wavelength measurement works on the principle that the absorbance ratio at two spectral points, λ_1 and λ_2, correlates with the concentration of the analyte of interest.[115] It demonstrates increased measurement rapidity, simplicity, selectivity, and sensitivity over conventional spectrophotometry.[116]

Several factors determine the selection of appropriate λ_1 and λ_2. In blood oximetry, 660 nm and 940 nm wavelengths are typically chosen as λ_1 and λ_2. This selection is partly because HbO and HbR have inverted absorption strengths at 940 nm compared with 660 nm. Several additional factors have resulted in the selection of 940 nm than 660 nm, including the availability of light sources and low absorption by the tissue and blood in the red and near-infrared ranges. It is worth noting that the recent technological progress in the availability of LEDs has opened the possibility of oximeters at wavelengths other than the traditional 660/940 nm. For example, 665/894 nm, 780/808 nm and 761/818 nm.[109] The primary motivation behind operating at these alternative wavelengths is reducing the scattering variability and accounting for other blood pigments.

3.2.2. The general selection criteria for operating wavelengths. The optimal selection of operating wavelengths (λ_1 and λ_2) for dual-wavelength measurements utilizes three specific operating regimes: isosbestic point, absorption foot, and the absorption peak.

Peak and isosbestic absorption points. The isosbestic wavelength is commonly used as a reference wavelength.[115] Any changes in peak absorbance due to the reagent of interest (x in our case) can be correlated with its concentration by computing the absorbance ratio. eqn (3) can be reduced to eqn (4) to facilitate the extraction of the concentration of the reagent of interest.

$$\lambda_2 \rightarrow \text{Isosbestic} \Rightarrow \begin{cases} A_{\lambda_1} = \varepsilon_{x,1} \times C_x \times t + \varepsilon_{y,1} \times C_y \times t \\ A_{\lambda_2} = K_{x,2} + K_{y,2} \end{cases} \tag{4}$$

Peak and foot absorption points. Beyond using an isosbestic wavelength, when the absorption spectrum of the analyte of interest exhibits both a maximum point (peak) and a minimum point (foot), the two can be taken as the target wavelengths. If the absorbance at the foot is negligible, then eqn (3) can be reduced to eqn (5). Any change in absorbance at the peak due to the reagent of interest can be correlated with its concentration. Indeed, this approach forms the basis of optimal wavelengths selection for bilirubin measurement. It can be noted that bilirubin has an absorption peak and foot at ~470 and ~530 nm, respectively. The illustrations

and the spectral data of the isosbestic, peak and foot absorption points are given in.[117,118]

$$\lambda_2 \rightarrow \text{Absorption foot} \Rightarrow \begin{cases} A_{\lambda_1} = \varepsilon_{x,1} \times C_x \times t + \varepsilon_{y,1} \times C_y \times t \\ A_{\lambda_2} = \varepsilon_{y,2} \times C_y \times t \end{cases} \tag{5}$$

Inverted absorption strength. Suppose a mixture has reagents such that the absorbance increases at one wavelength while decreasing at the other. In that case, the concentration variation can be obtained by computing the absorbance ratio or difference. This approach has been extensively used in pulse oximeters. 660 nm and 940 nm wavelengths are chosen for the simple reason that oxygenated haemoglobin absorbs more at 940 nm than at 660 nm, while the reduced haemoglobin absorbs less at 940 nm than at 660 nm.

3.3. Case study: application of dual wavelength in pulse oximetry

DWL spectrophotometry is widely known in pulse oximetry for measuring SaO$_2$. It involves comparing light absorbances of HbO and HbR at two wavelengths and analyzing the pulsatile component of arterial blood. Light is shined onto or through the tissue, usually the finger, followed by reflectance or transmittance measurements. The arterial pressure and diameter increase sharply during heart contractions and decrease when the aorta valve is closed. It can be noted that a blood vessel is elastic; thus, its diameter is expected to vary proportionally with heartbeats. The magnitude of the resulting optical signal can be correlated with SaO$_2$ since the non-pulsatile component stays constant and will not affect the measurement. Fig. 4a shows that only pulsatile blood flow is taken advantage of by tracking the associated variations in the absorbance readings.[119]

Hb molecules are responsible for oxygen transport from the lungs (high oxygen tension) to the tissues (low oxygen tension). SaO$_2$ is thus referred to as the per cent ratio of HbO to the total haemoglobin (HbO and HbR) concentration as defined in eqn (6). The average SaO$_2$ is approximated at 96–98% (arterial SaO$_2$) and 75% (venous SaO$_2$) in healthy adults depending on heart rate and oxygen partial pressure of the inhaled air.[120]

$$\text{SaO}_2 = 100 \times \frac{[\text{HbO}]}{[\text{HbR}] + [\text{HbO}]} \tag{6}$$

Considering the absorption spectra of chemically non-reactive HbO and HbR and based on the skin vasculature, longer wavelengths, red and near-infrared (NIR) light are used. Red and NIR can profoundly penetrate the cutaneous tissue and reach the dermal and subdermal layers where arteries and arterioles are located.[121] Besides, HbO absorbs more NIR than red light, while HbR absorbs more in the red than in the NIR region, as shown in Fig. 4b. Therefore, by combining eqn (3) and (6), the SaO$_2$ yields eqn (7) where ε is the extinction coefficient.

$$\text{SaO}_2 = \frac{100 \times \mathbb{R}\varepsilon_{940\text{nm}}^{\text{HbR}} - \varepsilon_{660\text{nm}}^{\text{HbR}}}{\mathbb{R}\left(\varepsilon_{940\text{nm}}^{\text{HbR}} - \varepsilon_{940\text{nm}}^{\text{HbO}}\right) - \left(\varepsilon_{660\text{nm}}^{\text{HbR}} - \varepsilon_{660\text{nm}}^{\text{HbO}}\right)} \Big\|_{\mathbb{R} = \frac{\text{AC\_660nm/DC\_660nm}}{\text{AC\_940nm/DC\_940nm}}} \tag{7}$$
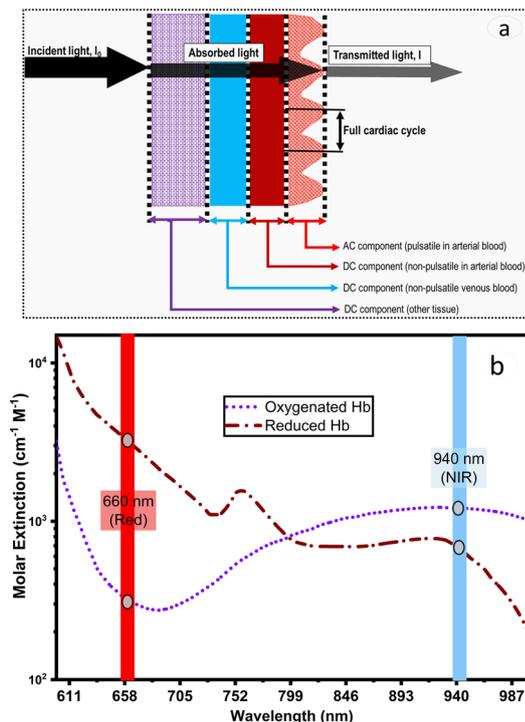
Fig. 4 (a) Illustration of pulsatile and non-pulsatile components in pulse oximetry. The pulsating blood helps distinguish between blood and tissue absorption in oximetric measurement. (b) Illustration of wavelengths selection for a pulse oximeter.

3.4. Dual wavelength as a means for bilirubin concentration measurement

3.4.1. Absorption properties of bilirubin. Bilirubin is a chromophore responsible for jaundice and does not absorb in the green, yellow, and red spectral range, as shown in Fig. 5a. Notice in Fig. 5b and c that bilirubin overlaps with other blood pigments, including Hb, lipid and melanin.[5] The absorption coefficient μ_a of bilirubin can be obtained from eqn (2). By considering the normal adult bilirubin levels as 1.2 mg dL^{-1} ($\sim$20 µmol L^{-1}) and the peak molar absorptivity as ε_{460nm} = 53 846 cm^{-1} M^{-1}, the absorption coefficient yields μ_a = 53 846 × 20.5 × 10^{-6} × 2.3 = 2.5 cm^{-1}.

3.4.2. Choice of optimal wavelengths for bilirubin monitoring. As mentioned above, Beer's law is based on the concept that the sum of absorbed and transmitted photons equals the incident photons. This law is insufficient in media such as blood with significant reflectance or scattering. Fig. 5d shows that scattering in the blue range ($\sim$470 nm) is around four orders of magnitude higher than the absorption in the red and infrared range (above 600 nm). However, Beer's law, hence DWL, can be used as an approximation to minimize scattering and other interfering background noise.[114,122]

As shown in Fig. 5 (a to c), bilirubin exhibits its highest optical activity in the blue region, where its optical spectra overlap with Hb's, lipid's and melanin's. Also, its molar extinction is higher than HbO's between 452 nm and 488 nm,

as evidenced by the BR-to-Hb extinction ratio; Fig. 5b and inset. Given that 470 nm is the peak for BR-to-Hb extinction ratio and has a relatively low absorption for HbO; and that 530 nm is an isosbestic point for HbO and HbR and has negligible absorption for BR; λ_1 and λ_2 can be selected as 470 nm and 530 nm, respectively. Hence eqn (3) yields eqn (8).

$$\begin{cases} A_{470} = (\varepsilon_{BR,470} \times C_{BR} + \varepsilon_{Hb,470} \times C_{Hb}) \times t \\ A_{530} = (\varepsilon_{BR,530} \times C_{BR} + \varepsilon_{Hb,530} \times C_{Hb}) \times t \end{cases} \Leftrightarrow R = \frac{A_{470}}{A_{530}} \text{ ap}; C_{BR} \bigg\|_{\varepsilon_{BR,530} \to 0}$$

(8)

3.4.3. Optimal path length and concentration for bilirubin absorption measurement. Looking back at the expression of Beer's law shown in eqn (1) and (2), the absorbance is dependent on the concentration of the substance of interest and the path length. These two parameters are critical for the reliability of the bilirubin concentration measurement. A series of theoretical simulations were carried out and have shown that a path length of not more than 0.3 mm is adequate for the measurement, and the results are summarized in Fig. 6 (a to d). These simulations are shown at the already determined analytical and reference wavelengths. Also, notice that the concentration range covered was 1.2–50 mg dL^{-1}, which corresponds to the pathophysiological levels projected from healthy individuals (1.2 mg dL^{-1}) to cirrhotic patients (50 mg dL^{-1}).

The theoretical spectral distribution of blood at varied bilirubin concentrations is shown in Fig. 6a. As can be seen on the whole spectral range, the variation in bilirubin concentration is not as obvious, except for the blue range where bilirubin exhibits the highest optical absorption (see inset of Fig. 6a). Furthermore, the relationship between optical attenuation by a blood sample with path lengths up to 1 mm is shown in Fig. 6b. These values were computed using the expression of Beer's law in eqn (1). Noticeably, 0.2 mm path length results in attenuation up to about 5%. Large path lengths result in high absorption and low incident light intensity on the optical detector, leading to low transmittance values. In spectroscopic terms, a transmittance (T) of more than 10% (*i.e.*, absorbance <1.0) is favourable, a transmittance between 1% and 10% (*i.e.* 2.0 > A > 1.0) is acceptable and in some cases, a transmittance between 0.1% and 1% (3.0 > A > 2.0) is allowed. Thus, path lengths below ∼300 µm are suitable for transmittance measurements at 470, and 525 nm and 0.2 mm path length can be used for optical measurements in the blood (Fig. 6b). Also, notice that using infinitely shorter path length is inappropriate as it may result in less effective measurement and produce unreliable results.

A comprehensive assessment of Beer's law at the operating wavelengths (470 and 525 nm) is provided in Fig. 6(c and d). It was done by normalizing the incident light I$_0$ at 100 and determining the transmittance (*i.e.*, the absorbance) under 300 µm path length. The comparison of the absorbance of bilirubin-blood shows that the change in bilirubin concentration is greatest at 470 nm. The absorbance
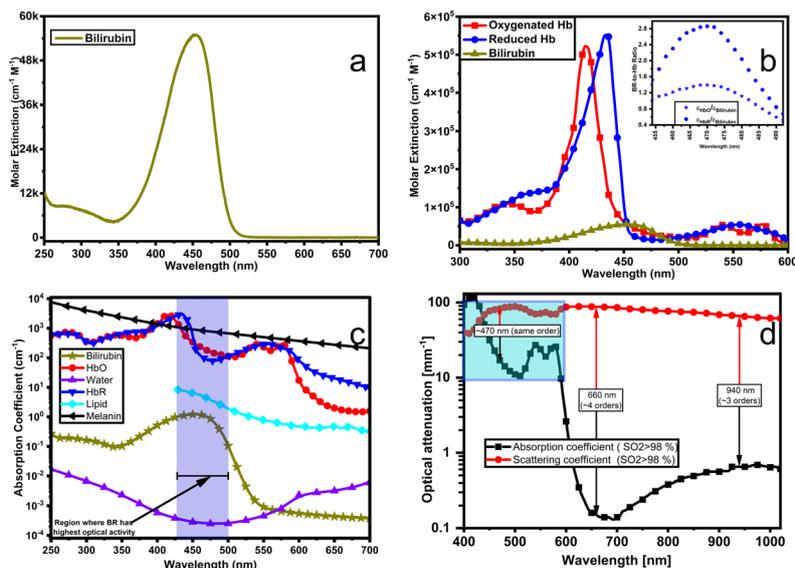
Fig. 5 (a) Spectral distribution of the extinction coefficients for bilirubin. (b) Comparison of molar extinction spectra for bilirubin, HbR and HbO. The inset shows molar extinction ratios (BR-to-Hb ratio). Molar extinction coefficients for BR, HbR and HbO are obtained from ref. 1. (c) Absorption spectra for bilirubin and other major chromophores (absorbing agents) in biological tissues: OxyHb and DeoxyHb at ~150 g L^{-1} in blood, lipid at 20% (v/v), water 80% (v/v), melanin at 14.3 mg mL^{-1}, and bilirubin at 1.2 mg L^{-1} in blood.[5] (d) Absorption and scattering coefficients spectra for the whole blood with 98% oxygen saturation; adapted from ref. 8. Scattering coefficients are ~4 orders of magnitude higher than the absorption coefficients at wavelengths above 600 nm but have the same order of magnitude on a [450–590 nm] interval.
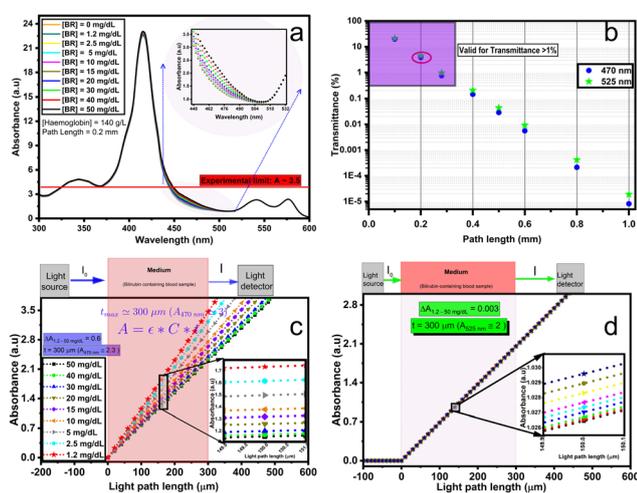

Fig. 6 (a) Distribution of the absorption spectra for blood at varied bilirubin concentrations. (b) Relationship between attenuation by blood sample with path lengths up to 1 mm. (c and d) Approximation of Beer's law for a blood sample at varied bilirubin concentrations obtained from theoretical data. At 300 μm path length, the transmittance values (*i.e.,* the absorbance) were obtained for (c) 470 nm and (d) 525 nm.

difference is 0.6 at 470 nm compared to 0.003 at 525 nm, corresponding to over two orders of magnitude.

3.5. Bilirubin photodegradation as a means of bilirubin levels measurement

As described in section 1.3, phototherapy involves illuminating blue light on an infant's skin, resulting in the disappearance of bilirubin (UCB) from the body *via* excretion

of the hydrophilic byproducts. Inspired by phototherapy, the correlation between degradation parameters and irradiation times can be used to estimate bilirubin levels.

This subsection suggests a quantitative measurement of bilirubin using its degradation kinetics. Several optical aspects of bilirubin degradation have been studied, including peak area, concentration, absorbance, and more.[123] These studies have demonstrated that the degradation parameters can be correlated with irradiation doses and concentrations.

Like many chemical and biochemical reactions, the photodegradation reactions follow fixed order kinetics, and the order number n is not always an integer.[124] The accurate assessment of the effects on bilirubin illumination requires information on its degradation mechanisms, which is crucial in determining its fate. Various fate models have been suggested to fit the degradation pathways of bilirubin,[125–127] and the models are shown in eqn (9)–(11).

eqn (9) constitutes the first-order pseudo-kinetics characterized by exponential decays and always represents a relationship between the absorbance or concentration and time.[124] It has been shown that the photodegradation of bilirubin follows this reaction type.[125] Indeed, this has been chosen to model the degradation process due to its simplicity and straightforwardness. No comparative study about the effectiveness of the models has been found. *A*: bilirubin absorbance, A_{coeff}: bio-photodegradation coefficient, *k*: bio-photodegradation rate constant, *t*: irradiation time.

$$\frac{\mathrm{d}A}{\mathrm{d}t} = -k \times A(t)$$
$$\Downarrow$$
$$A(t) = A_{\text{offset}} + A_{\text{coeff}}\mathrm{e}^{-k \times t}$$

(9)

Proposed by Dubin et al.,[126] eqn (10) consists of a multi-order rate reaction. Dubin suggested that the photodegradation of bilirubin can be modelled using dual order kinetics comprising the first and second orders.[126]

$$\frac{dA_t}{dt} = -\frac{k}{A_0} \times A_t^2$$
$$\Downarrow$$
$$\frac{1}{A_t} = \frac{1}{A_0} + \left(\frac{k}{A_0}\right) \times t \qquad (10)$$

It is widely recognized that bilirubin degradation results in three major byproducts, including lumirubin, biliverdin and other isomers.[128] Thus, the eqn (11) shows that its kinetics can be expressed as fractional pathways leading to a multi-exponential model.[127]

$$A_t = A_{offset} + \sum_{i=1}^{n}\left(A_{i,coeff} e^{-k_i \times t}\right)$$
$$\Downarrow$$
$$A_t = A_{offset} + A_{1,coeff} e^{-k_1 \times t} + A_{2,coeff} e^{-k_2 \times t} + A_{3,coeff} e^{-k_3 \times t} \qquad (11)$$

Section 3.4 above has extensively described the DWL approach for bilirubin monitoring. Thus, the utility of both DWL and photodegradation-based bilirubin estimation can be applied to increase the sensor capability to produce more accurate and reliable results.

3.6. Evaluation of potential sources of errors

As described above, dual wavelength is a potential spectrophotometric approach for detecting slight variations in the absorption of bilirubin in the blood. However, multiple sources of error exist that lead to a false interpretation of BR levels; these range from a patient's pathological parameters to measurement and device constraints. The following segment describes potential sources of error and suggests some corrective interventions to increase the reliability of BR measurement. Also, notice that the reported errors represent the worst-case scenarios in dual-wavelength measurements.

3.6.1. Oxygen saturation (both *in vivo* and *in vitro*). It has been reported that the SaO_2 can be affected by physiological and pathological parameters. These may include cirrhosis,[129] body temperature,[113] physical exercises,[130] or cardiorespiratory conditions.[131] These parameters may also lead to an over or underestimation of BR levels due to a surge in SaO_2. The latter could be corrected by applying a multiwavelength approach that uses multi-dimensional solutions to Beer's law to compensate for SaO_2. It can also be corrected by choosing a different reference wavelength, such as 540 or 576 nm, that manifests an absorbance variation similar to that at 470 nm (see Fig. 7a and b). It has been reported that SaO_2 can go as low as 90% in most adult patients.[132] The effect of SaO_2 variability on the absorbance ratio was studied, and the associated uncertainty error is shown in Fig. 7e.

3.6.2. Dysfunctional haemoglobin (both *in-vivo* and *in-vitro*). There are two major dysfunctional haemoglobin forms: carboxyhaemoglobin (COHb) and methaemoglobin (MetHb). These forms possess distinct aberrant spectral signatures than oxyhaemoglobin and deoxyhaemoglobin. Although they exist in the blood at low concentrations, they may cause inaccurate and false interpretations of bilirubin levels.[133,134] A multiwavelength approach can also be used to address this. It has been reported that acceptable blood levels for both MetHb and COHb are 2%.[135] The effect of the variability in MetHb or COHb blood levels was studied (as shown in Fig. 7e). Changes in the concentration would result in average estimates of ±2.3 mg dL⁻¹ and ±1.09 mg dL⁻¹, respectively for MetHb and COHb.

3.6.3. Spectral variability of light sources (both *in-vivo* and *in-vitro*). LEDs are not monochromatic sources as they exhibit a spectral emission range usually ~25 nm at 50% of the maximum for blue and green. Moreover, their emission spectrum is temperature-dependent, resulting in spectral broadening or peak shifting.[136] This spectral variability would lead to the variation in absorption coefficients of BR, HbR and HbO, resulting in the measurement error. The effects of spectral variability were studied by comparing the impact of an LED and a laser diode (LD); an LED stands for a broader spectrum and an LD for a single wavelength. This is achieved by integrating the absorption coefficients of a blood sample at varied bilirubin concentrations (0.15–50 mg dL⁻¹) over wavelengths occupied by the LED's relative spectral power. The obtained absorbance ratio (DWL) sensitivity was ~0.001 per mg dL⁻¹ for LED and LD, as shown in Fig. 7c. Thus, compared to LD, the spectral variability for LEDs would not result in any discernible measurement error.

Beyond the emission spectra broadening, the operating temperature of the LEDs would also impact the emission spectrum (mainly peak shifting). The effect of temperature on the peak wavelength shifting was also investigated for blue, green, amber and red colour LEDs using a 4 K temperature change (see Fig. 7d). Notice that 4 K was selected as the largest possible variation in body temperature. Analyses show that a change of 4 K would result in an average BR concentration variation of ±0.82 mg dL⁻¹ (see Fig. 7e). These suggest that the LEDs are well suited for use as a light source in the optical measurement of BR.

3.6.4. Fibrosis formation (for *in vivo* only). In the case of implantable bilirubin monitoring devices, the body response implant becomes an important consideration. The body may recognize an implant as foreign through fibrosis by covering it with scar tissue, negatively impacting the optical measurement. This can be corrected by carefully selecting a packaging material based on biocompatibility and bio-inertness. Studies have shown that scattering coefficient; μ_s (λ), are much higher than absorption coefficients; μ_a (λ), in scar tissues and can be estimated as $\mu_{a, 470nm} = 0.338$ mm⁻¹, $\mu_{s, 470nm} = 1.836$ mm⁻¹, $\mu_{a, 525nm} = 0.270$ mm⁻¹, $\mu_{s, 525nm} = 0.973$ mm⁻¹, $\mu_{a, 576nm} = 0.248$ mm⁻¹, $\mu_{s, 576nm} = 0.944$ mm⁻¹.[137] In the study by Lichter et al.,[138] a fibrous encapsulation of up to ~70 μm thick was observed on the diamond after 15 weeks of implantation. As shown in Fig. 7e,
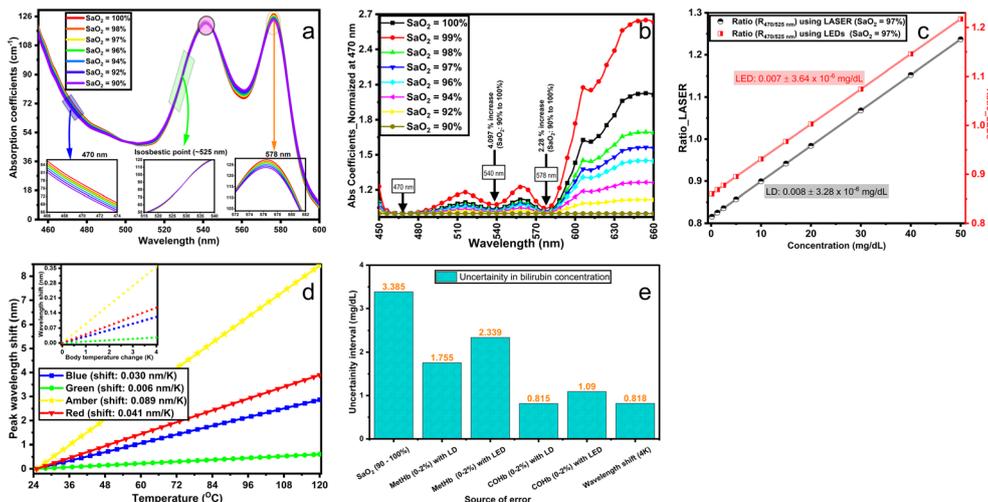
Fig. 7 (a and b) Illustration of optimal selection for specific wavelengths at varied SaO$_2$ (90–100%) for a multi-wavelength approach standardized at 470 nm. Absorption coefficients used are for haemoglobin and were obtained from ref. 1. (c and d) Investigation of the effect of the spectral variability in optical sources. Part c compares the impact of an LED's broader spectrum and LD's narrow spectrum on the device sensitivity. Red stands for the absorbance ratio considering the impact of the LED's spectrum and black for a single wavelength. Part d illustrates the shift in the dominant wavelength as a function of temperature for a multi-colour LED LZ4-00MA00 RGBA LED (LED Engin. Inc). (e) The summary of the uncertainty error values for the worst-case scenarios. These values imply that the concentration of bilirubin [BR] can be expected in the range [BR] ± error mg dL^{-1}.

the formation of fibrous tissue, 70 μm thick, would result in an error of ± 3.2 mg dL^{-1}. It should be noted that this is a worst-case error estimate as it does not account for pulse-based measurement.

3.6.5. External optical interference (both *in vivo* and *in vitro*). The spectral response of silicon photodetectors extends from visible to NIR range (usually 400–1200 nm), and any light other than the wavelengths of interest would inevitably result in a measurement error. Implementing an optical filter, applying an ambient light cancellation algorithm or carefully mounting the sensor (photodetector – LED) system could result in a reduced uncertainty error.[139] Alternatively, modulating the optical emitters at a specific frequency (10's kHz) and tuning the detector to that same frequency would make it relatively insensitive to ambient light or other optical interferences.

4. Conclusions and future outlook for bilirubin monitoring

4.1. New bilirubin monitoring systems for real-world applications

This section suggests and discusses the implementation of three devices that utilize the DWL or photodegradation kinetics approaches to determine bilirubin levels. At the heart of each device, an MCU processes data and controls all operations from LEDs driver to data acquisition. However, the discussion is limited to the functional and engineering aspects since we aim to give a perspective rather than implement a product readily available for commercial use. The PoC systems presented herein may be employed for *in vitro* and *in vivo* measurements of blood bilirubin levels.

4.1.1. *In vitro* homecare bilirubin meter. A homecare bilirubin meter (HBM) is proposed. It consists of an *ex vivo* point-of-care blood BR testing kit that can be similarly used at home to a blood glucose test with finger pricks. A simplified functional block diagram for HBM is shown in Fig. 8a. It incorporates a light sensor system (LEDs, a photodiode, and probes), analog front end (AFE), analog-to-digital converter (ADC), an MCU and a display system. LEDs are driven alternately, and light is transmitted through or reflected by the sample to the photodiode. The photodiode then converts light into an electrical signal which is conditioned and sent to an ADC for digitization and then to the MCU for processing. A data processing algorithm implemented in an MCU then computes BR concentration by comparing the intensities of the two signals generated by both wavelengths (470 and 525 nm in this case). The final stage involves data acquisition and display on a digital readout. The system could include a communication link with smartphones and a cloud data accumulation for analytical purposes.

Although HBM should in practice be a simple device, its implementation requires a careful design assessment of light sources, photodetectors and mixed-signal electronics. It should be noted that drive currents should be sufficient to provide a proper optical signal yet appropriate to minimize any temperature-dependent wavelength shifts, spectral broadening, and unwanted photobleaching of bilirubin.

Lighting systems. Light can be produced *via* several modes, including electric discharge, incandescence, photoluminescence, and electroluminescence.[140] Electroluminescence exhibits extensive emission efficiency, narrow spectral bandwidth, excellent drive characteristics, low electrical power requirements, higher optical power
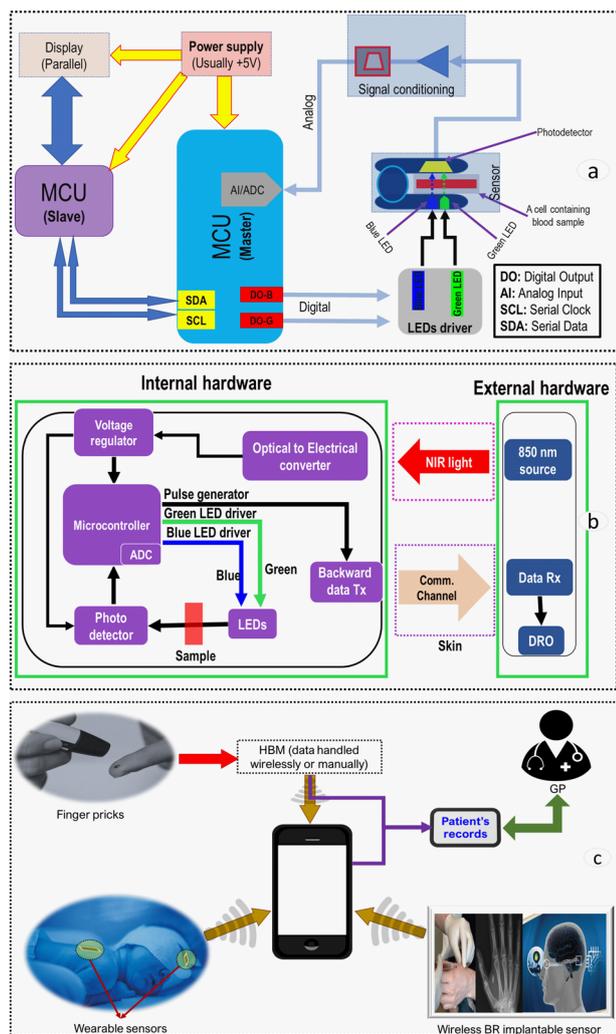
Fig. 8 Block diagram of a homecare device and implant. (a) Homecare bilirubin meter: the system takes an input analog signal, scales it and feeds it to an MCU *via* an ADC. Data is processed and then sent to data acquisition and display unit. (b) Bilirubin implantable sensor: the NIR source illuminates the PV cell (optical to the electrical converter), which acts as a power supply. The MCU is programmed to drive the LEDs. Blue and green LEDs are triggered to switch on and off. The internal device communicates with the external *via* an optical wireless or radio frequency communication link. (c) Illustration of the three highlighted BR devices and their interactions with medical/clinical personnel.

output, faster-switching speed, and higher signal-to-noise ratio compared to several other sources.[139,140] Although laser diode (LD) exhibit narrower spectral bandwidth than LEDs and have been used in pulse oximeters,[141] LEDs merit consideration due to their lower electrical power requirements, smaller footprint, off-the-shelf availability, lower cost and mounting easiness. The wall-plug efficiency of a LASER diode is still below 40%, which is much lower than LED's that can reach above 80%.[142] Thus, when a LASER source is used in an implant, both energy consumption and heat generation should be carefully monitored. Besides, laser

sources require compliance with established safety standards and regulations.[143]

Photodetectors. The choice of an optical detector depends on factors like footprint size, spectral responsivity, transient response, and optical power output linearity. Photodetectors are used to sense the intensity of light emitted by the LEDs after being backscattered or transmitted through the blood sample. Various schemes can be used as photodetectors, including photoelectric cells, phototransistors, photodiodes, and photo ICs.[144] Silicon photodiodes have been used in most optical sensors such as pulse oximeters[144] and should be preferred for bilirubin estimation applications.

Probes and setup. Several parameters should be considered to maximize the measurement accuracy, including optical path length, probes alignments, LED-photodiode-tissue spacing and other signal distortion-related factors (reusability or disposability of probes). LED-PD separation up to 12 mm (~finger's diameter) for pulse oximeters has been used in transmission mode.[145] However, a path length as low as 200 μm should be used for a BR sensor to obtain a valid optical signal as evidenced by a ~5% transmittance through a bilirubin-containing blood sample (see Fig. 6). In reflectance mode, it has been reported that <5% of incident light is backscattered, and the intensity drops with the square of the distance.[146] Thus, LEDs and the photodiode should be in a direct contact with a blood sample to maximize optical detection and SNR.[147] However, a drawback for small spacing is optical shunting[145] and could be resolved by inserting a barrier between an LED and a photodiode.[148]

Analog front-end (AFE). AFE includes a transimpedance amplifier (TIA) that maximizes the SNR by amplification, offset cancellation, self-calibration, filtering, and current-to-voltage conversion before being passed onto the ADC. Several techniques, such as fully differential TIA[149] equipped with correlated double sampling (CDS) circuit and switch capacitors, could be used for a significant increase in resilience against noise and background light. It has been reported that the optimal bandwidth for pulse oximeter filters is 0.6–15 Hz,[150] and as such, a passband filter can be utilized. A 50/60 Hz notch filter for powerline noise or a low-pass Butterworth filter for ambient and LED switching noise have been implemented in pulse oximeters[151] and could also be utilized. Higher-order filters could be used to improve accuracy, but this requires an additional power source and board space.[151] Typically, digital signal processing tools are used to remove frequencies below 0.6 Hz. For a bilirubin measurement device, a similar measurement frequency range is required. This would allow isolating the contributions of transient arterial blood absorption from the constant background absorption by the tissue. Additionally, 60 Hz or 120 Hz signal components are usually generated from indoor lighting and other artificial optical sources and should be mitigated.[152]

Signal conversion. An ADC converts amplified analog signals to digital series of bits in order to be processed by an MCU. The ADC's choice depends on resolution, accuracy

(assessed by quantization noise and SNR), and sampling rate. A lower resolution results in increased quantization noise (±1/2 LSB), whereas higher resolution results in an exponential increase in power consumption and die size.[153] If a 10-bit ADC with a 0 to 5 V input range is opted for, signals would be quantized in 1024 codes of ~4.88 mV each as highlighted in eqn (12) (LSB: lowest significant bit, FSR: full-scale range, n: ADC resolution). If the BR concentration increases from 0.15 mg dL^{-1} (health person) to 50 mgdL (cirrhotic patient), this may take up to 50 mV (~10 levels) equivalent to 1% of the 10-bit ADC dynamic range. This results in a significant equitization error, which can be addressed by using (a) higher resolution ADCs and/or (b) analog circuits that enable subtracting the non-bilirubin components before conversion and exploiting a larger portion of the ADC dynamic range.

$$1\ \text{LSB} = \frac{\text{FSR}}{(2^n - 1)} \quad (12)$$

Microcontroller/microprocessor. The MCU selection criteria include power requirements, clock frequency, data bus width, data or program memory size and type, communication interface type and the number of I/Os. 8-bit data bus width PIC MCUs have been extensively used to date.[154] The MCU generates all control signals to the input, output, memory, and communication peripherals. An algorithm should be implemented to identify individual photo signals and compute the ratio, which should, in principle, correlate with bilirubin levels. Digital filters such as FIR filters have been implemented successfully in pulse oximeters[154] and could be exploited in bilirubin sensors. An algorithm could also be implemented to compensate for errors associated with non-bilirubin features such as temperature, dysfunctional Hb forms or SaO_2 by dynamically adjusting LED's drive current *via* a feedback control loop. Depending on system needs, an optimal choice of data communication protocol should be made between serial and parallel communication or a hybrid of both. Nonetheless, serial communication protocols including I2C or SPI are preferred due to their simplicity and lower resource requirements.[155] A comparison of selected communication protocols (UART, SPI and I2C) is shown in Table 4.

4.1.2. Minimally invasive implantable bilirubin monitoring sensor. The simplified block diagram of the proposed implantable sensor is shown in Fig. 8b. The sensor utilizes the DWL approach for bilirubin monitoring and incorporates both the external and internal parts. The internal part comprises an optical transducer, sensor system (described in sections 4.1.1), a wireless transmitting unit, an ADC and an MCU. Low power consumption and integrated analog circuits are two desired key features for an MCU in an implant; these can significantly reduce the number of components and, ultimately, the device's size. The MCU with built-in ADCs and enhanced analog parts, including the integrated configurable TIA, general-purpose analog output, and configurable digital I/O port supporting multiple communication protocols, is preferred.

The MCU can drive the LEDs directly without other peripheral components. The photo signal from the photodiode can then be sent to the TIA and configurable amplifiers in the MCU and digitalized by the internal ADC. There is no signal processing process performed in the MCU to keep the lower power consumption of the internal device. In turn, the acquired data is transmitted *via* skin tissues to the receiving end on the external hardware, where another MCU will do further processing. Then a numerical index corresponding to bilirubin concentration is computed and displayed. The following discusses the implant's key features.

Power delivery. Continuous and safe power delivery across the skin is a key requirement for an implant. Common methods include batteries, percutaneous plugs, inductively coupled coils, and optical power delivery. Batteries and coil-based methods can be used for low power prostheses; however, they are not viable in applications with dimension constraints.[158] Percutaneous plugs require wires to cross the skin, increasing the risk and potential for infections.[159] On the other hand, optical power delivery is safer;[160] however, extra care should be taken since the safety depends on various factors that can be detrimental if unaddressed. These factors include the transducer's external quantum efficiency (EQE), skin loss, package material loss, and maximum permissible exposure (MPE). Refer to Fig. 9a to c for a graphical representation of these factors. The analysis of the effect of EQE, optical losses, MPE, open-circuit voltage, and fill factor reveals that crystalline Si-based cells achieve the best output power density at ~1000 nm, Fig. 9d. Additionally, organic photovoltaic cells are deemed inadequate for implantable devices due to their low efficiency and poor environmental stability.[161]

Backward data transfer. A stable, continuous, and safe means of back data transfer across the skin is a key requirement for an implantable bilirubin sensor. Wireless communication (RF and optical) is preferred over

Table 4 Comparison between various communication protocols

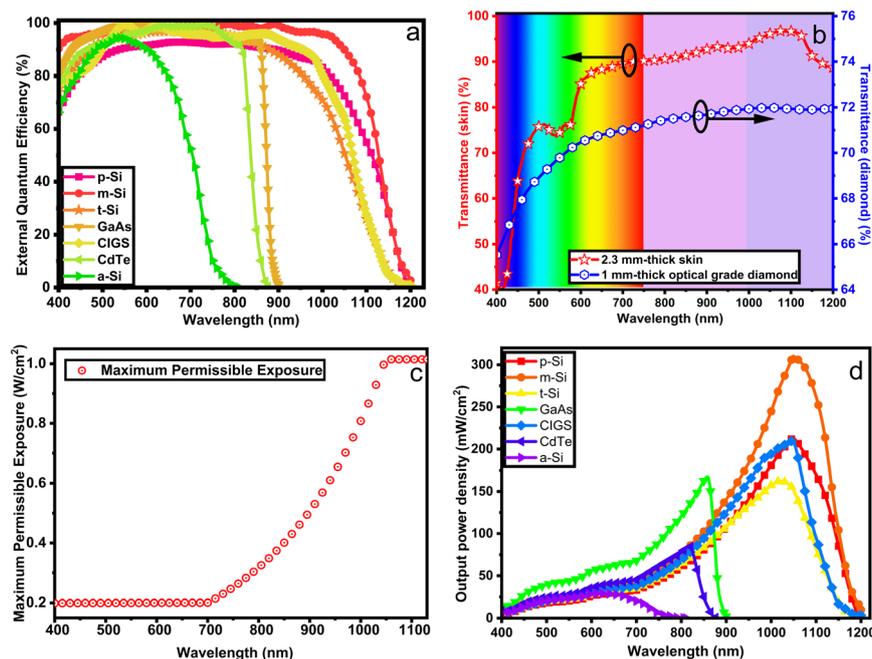|	UART	I2C	SPI
Complexity	Simple	Easy to communicate several devices	Complexity increases with device count
Speed	Slow	Faster than UART	Fastest of all
Device count	Two devices at maximum	127 devices at maximum	Many
Wire count	One	Two	Four
Duplex	Full duplex	Half-duplex	Full duplex
Slaves-to-masters	One to one	Several masters and slaves	One master, many slaves

Fig. 9 Characterization of key features of an implantable bilirubin sensor. (a) The external quantum efficiency of common PV cells; adapted from ref. 3. (b) Optical transmittances of a 1-mm optical grade diamond; adapted from ref. 4 and a 2.3 mm-thick skin; adapted from ref. 7 where ~2.3 mm is the average skin thickness.[9] (c) Maximum permissible exposure of the skin; adapted from ref. 11. (d) Estimated PV cell output power density after accounting for the EQE, MPE and diamond and skin losses. The highest power density is identified in m-Si PV cells on the [900–1100 nm] interval. m-Si: monocrystalline silicon, p-Si: polycrystalline silicon, t-Si: thin-film transfer silicon, a-Si: amorphous silicon, GaAs: gallium arsenide, CIGS: copper indium gallium selenide, CdTe: cadmium telluride.

percutaneous wires to minimize the risk of infections. A wireless multimodal transceiver has been reported.[162] Using a single PV cell, a bidirectional data transfer and power delivery mechanism could benefit medical implants with small size and achieve both energy harvest and data transceiver with only one component.

Placement site. The optimal implant placement location is a critical device constraint and should offer low-fat levels and adequate blood volume. Some potential placement means, and sites include the lobule of auricle, foreleg (tibialis anterior), forearm, purlicue (between finger and thumb), biceps, triceps and more. Preferably, it could be on top of the capillary bed in sites including lobule of auricle, wrist or the space between the index finger and the thumb for their adequate implant vasculature. However, the most optimal site would be the foreleg (tibialis anterior) due to its soft-tissue motion, enough blood and ease to wrap with a digital readout.

Packaging material. One of the steps towards fabricating a wirelessly powered implant is to define the packaging material. It must be biocompatible, optically or RF transparent, bio-inert, thermally conductive, and must ensure a hermetic seal. Table 5 compares common implant biomaterials, including polymers, ceramics, metals and diamonds.

Biocompatibility. Polymers have a long history in biomedical applications, as exemplified by the use of ultra-high molecular weight polyethylene; UHMWPE, in hip replacement.[163] Silicon nitride has been used for medical implants.[164] Titanium has a good record as a biocompatible material due to its passive oxide layer.[164] Diamond has been used in orthopaedic implants for a long time with no adverse reaction in the body and is currently being used in bionic eye implants.[165,166]

Biochemical inertness. For long term implantation, the performance of polymers such as UHMWPE is compromised by low stiffness and creep compliance.[167] Most ceramic materials possess an inert behaviour.[164] Diamond is cleaned in a mixture of sulphuric and nitric acids at about 400 °C and without adverse effects; hence it can certainly sustain human vasculature, usually saline at 37 °C.

High thermal conductivity. The thermal conductivity is very high in UHMWPE thin films but low in bulky ones.[168] Ceramic materials[164] and titanium[169] exhibit lower thermal conductivity. Optical grade diamond has a high thermal conductivity,[4] implying that heat from electrical power dissipation would rapidly vanish to the body in a spatially uniform fashion. This eliminates the formation of hotspots that may otherwise result in tissue damage and avoids electronic components damage due to overheating.

Optical transparency and absorption. UHMWPE exhibits less than 10% optical transmittance in the 400–900 nm spectral range.[170] Most ceramics are not transparent to visible or NIR light, but diamond is weakly absorbing in the [500–1000 nm] region with an optical transmittance of over 71%.[4]

Table 5 Common biomaterials for implants.[156,157] Diamond is the best candidate

	Usage	Thermal conductivity [W K^{-1} m^{-1}]	RF absorption	Optical absorption	Hermeticity
Polyethylene	Hip replacement	~0.2	Low	Partial	✓
Parylene-C	Neural probes	Negligible	Low	Partial	✓
Silicon nitride	Chip-scale package coating	~90	Low	Low	✓
Silicon carbide	Chip-scale package coating	~12	Partial	Partial	✓
Alumina	Hip and tooth replacements	~30	Low	Partial	✓
Steel	Orthopedic implants, stents	~50	Significant	Partial	✓
Titanium	Pacemakers, cochlear	~26	Low	High	✓
Diamond	Bionic eye	>2000	Low	Negligible	✓

Hermeticity. A hermetic seal for polymers can be created using epoxy, but tissue motions against the epoxy could produce wear particles leading to device failure.[171] The LASER welding technique has been used for sealing titanium substrates.[172] A hermetically sealed diamond package can be created by gold braze LASER welding[138] to avoid damage to the electronics due to moisture ingress.

4.1.3. Bilirubin wearable sensors for infants. Hyperbilirubinemia is a life-threatening condition for neonates, and its diagnosis requires a bilirubin test which is a routine in both provincial and tertiary referral hospitals. These diagnostic testing capabilities are not readily available in remote areas and for developing countries where healthcare resources are limited or inadequate, leading to delays in treatment. There is thus an urgent need to identify a reliable and affordable bedside and in-community bilirubin test to positively impact the lives of millions of infants worldwide by facilitating early interventions.

Jaundice phototherapy involves illuminating blue light on an infant's skin to treat hyperbilirubinemia. Along with phototherapeutic treatment, various testing techniques have since been in place and have been extensively used in clinical settings.[53] However, the advent of modern solid-state technologies (LEDs, photodiodes, transistors and MCUs)[173] is a game-changer towards device miniaturization and improved effectiveness or efficiency.

This subsection suggests a wearable sensor for quantitative bilirubin measurement by DWL analysis (Fig. 8c) in reflective mode. It consists of a noninvasive transcutaneous wearable sensor that can be placed on the infant's forehead, sternum, forearm, or back. Key design constraints and considerations, including optical and electronics systems, are identical to the described HBM and implantable bilirubin sensor.

Reports have demonstrated that the bio-photodegradation features can be correlated with bilirubin concentrations. As mentioned, these relationships suggest a direct quantitative bilirubin levels estimation. Consequently, the sensor can be integrated into the fabric worn during phototherapy as a secondary method for bilirubin monitoring and determination. In addition to DWL and photodegradation-based bilirubin estimation, extra LEDs (red and infra-red) can be integrated to increase the sensor capability for simultaneous measurement of bilirubin and other infants' vitals. These may include the heart rate, respiration, SaO$_2$, body temperature and blood pressure, which are critical signs of the infant's condition. The deterioration of any of these vitals could appeal to immediate clinical interventions. Thus, a device that can monitor these conditions could be a desirable diagnostic tool.

4.1.4. Bilirubin data collection and potential interventions. Testing blood BR is an essential part of cirrhotic patients' care plans. A patient may need to visit a doctor several times a year for formal testing depending on the disease severity. It is, however, essential to measure BR levels regardless of time or space since levels fluctuate throughout the day. Levels, evolution patterns, and relevant information may be logged and passed on to one's doctor (Fig. 8c). Based on this information, therapeutic interventions (outpatient visit, medication, or dose), physical (cardiac) exercises or dietary interventions may be suggested to prevent or prepare for complications. Various methods can be used for patient–doctor interactions.

Logbook method. Although manual recording (paper or computer-based) could bring awareness to high bilirubin levels, it may lead to data loss, entry errors and recall bias. Besides, the patient must take additional steps to report their information *via* email, SMS, chat, or call.

Wireless technologies. This process could provide more reliable data access by one's doctor. For example, the sensor could incorporate a Bluetooth scheme that channels data to a mobile app and shares this information with one's doctor *via* the internet to facilitate real-time support.

Graphical visualization. It could enhance the identification of trends in the data through examining patterns over extended durations but would easily confuse patients who are not familiar with graphs; nonetheless, verbal materials can be integrated for convenience.

4.2. Conclusions and future outlook

The goals of this review article are to (1) increase awareness of the detrimental impact of cirrhosis and hyperbilirubinemia on individuals, families and societies, (2) highlight the lack of appropriate diagnostic tools and the need for state-of-the-art methods, (3) outline the system-level constraints for real-world monitoring applications and (4) provide a perspective of future developments. We have revealed that the existing techniques for bilirubin measurement require lengthy clinical procedures, which result in extensive turnaround times. We have also

highlighted the need for a point-of-care bilirubin estimation technique to ensure round-the-clock monitoring of patients, provide early diagnosis, suggest preventive measures and treatment compliance, and improve prognostic outcomes.

A significant amount of scientific and clinical knowledge has been generated and gained about the bilirubin measurements for nearly a century. However, there is generally a lack of reliable, low-cost PoC capabilities that meet the needs of the 21st century. Besides, the potential for translating most academic research-based scientific techniques to clinical practices remains impractical, and the performance improvement for the existing clinical methods is impossible. The article lays out current scientific and clinical strategies, and some potential state-of-the-art techniques have been experimentally investigated, including dual-wavelength[117,174] and photodegradation kinetics.[175] Moreover, these works were conducted using phantoms and animal blood with normal residual bilirubin levels. However, it is still unclear whether the results can integrally be translated into clinical use. Therefore, future research should focus more on developing impactful systems for clinical use. Additionally, there have been tremendous research and recent development of several biosensing techniques that can be used to screen biochemical markers for the prognosis, diagnosis and management of diseases.[176] These techniques utilize various sensing approaches, including optical,[177] plasmonic,[178,179] photonic[180] and nanoparticle-based[181] approaches.

For instance, some bilirubin metabolic pathways are still controversial after nearly a century of research. New insights suggest that proportions of conjugated bilirubin are excreted *via* the renal system, as an alternative to intestinal excretion, even in normal physiological jaundice with no associated pathological concerns.[12] However, these levels are minimal, potentially at three orders of magnitude less than the normal total serum levels. Thus, the clinical relevance of this renal excretory pathway may be overwhelming. Whether or not bilirubin in urine holds diagnostic importance in screening for neonatal jaundice and cirrhosis is yet to be discovered. Therefore, research in bilirubin detection in urine could enormously benefit from these efforts in the future.

Author contributions

Jean Pierre: conceptualization, writing – original draft, data curation and formal analysis. Shiqiang, Genia, Kate, Terry, Zhangyu, Omid, Steven, and Arman: writing – review and editing. Steven and Arman: funding acquisition, supervision, and validation.

Conflicts of interest

SP is a shareholder in iBIONICS, a company developing a diamond based retinal implant. SP is a director and shareholder of Carbon Cybernetics, a company developing a carbon fibre based neural implant. AA is a shareholder in BrainConnect Pty Ltd, an Australian startup developing physiological and neurophysiological and interventional solutions for a range of neurological disorders. OK is a shareholder and currently the Managing Director at BrainConnect Pty Ltd.

Acknowledgements

Notes and references

1 S. L. Jacques and S. Prahl, *Biomedical optics (ECE532)*, 1998, **https://omlc.org/spectra/index.html**.

2 T. A. Mulaikal and J. C. Emond, in *Liver Anesthesiology and Critical Care Medicine*, ed. G. Wagener, Springer, 2018, pp. 3–19, DOI: **10.1007/978-3-319-64298-7**.

3 B. Minnaert and P. Veelaert, *Energies*, 2014, **7**, 1500–1516.

4 S. Coe and R. Sussmann, *Diamond Relat. Mater.*, 2000, **9**, 1726–1729.

5 J. Yao and L. V. Wang, *Laser Photonics Rev.*, 2013, **7**, 758–778.

6 G. W. Neff, C. W. Duncan and E. R. Schiff, *Gastroenterol. Hepatol.*, 2011, **7**, 661.

7 A. Bashkatov, E. Genina, V. Kochubey and V. Tuchin, *J. Phys. D: Appl. Phys.*, 2005, **38**, 2543.

8 N. Bosschaart, G. J. Edelman, M. C. Aalders, T. G. van Leeuwen and D. J. Faber, *Lasers Med. Sci.*, 2014, **29**, 453–479.

9 P. Oltulu, B. Ince, N. Kökbudak and F. J. T. P. Kılıç, *Turk. J. Plast. Surg.*, 2018, **26**, 56–61.

10 L. Ziberna, M. Martelanc, M. Franko and S. Passamonti, *Sci. Rep.*, 2016, **6**, 29240.

11 P. K. Upputuri and M. Pramanik, *J. Biomed. Opt.*, 2019, **24**, 1–20.

12 M. Thomas, W. Hardikar, R. F. Greaves, D. G. Tingay, T. P. Loh, V. Ignjatovic, F. Newall and A. E. Rajapaksa, *Clin. Chem. Lab. Med.*, 2021, **59**, 1025–1033.

13 D. R. Dufour, J. A. Lott, F. S. Nolte, D. R. Gretch, R. S. Koff and L. B. Seeff, *Clin. Chem.*, 2000, **46**, 2027–2049.

14 G. M. Hirschfield and G. J. Alexander, *Ann. Clin. Biochem.*, 2006, **43**, 340–343.

15 K. V. Williams, S. Nayak, D. Becker, J. Reyes and L. A. Burmeister, *J. Clin. Endocrinol. Metab.*, 1997, **82**, 1727–1733.

16 F. J. Farrell, E. B. Keeffe, K. M. Man, J. C. Imperial and C. O. Esquivel, *Dig. Dis. Sci.*, 1994, **39**, 2255–2259.

17 S. P. Roche and R. Kobos, *Am. Fam. Physician*, 2004, **69**, 299–304.

18 V. K. Bhutani, L. H. Johnson and R. Keren, *Pediatr. Clin. North Am.*, 2004, **51**, 843–861.

19 N. M. Blondet, D. J. Messner, K. V. Kowdley and K. F. Murray, in *Physiology of the Gastrointestinal Tract*, Elsevier, 2018, ch. 43, vol. 6, pp. 981–1001.

20 D. Schuppan and N. Afdhal, *Lancet*, 2008, **371**, 838–851.

21 J. L. Herrera and R. Rodríguez, *Gastroenterol. Hepatol.*, 2006, **2**, 124–133.

22 A. A. Mokdad, A. D. Lopez, S. Shahraz, R. Lozano, A. H. Mokdad, J. Stanaway, C. J. Murray and M. Naghavi, *BMC Med.*, 2014, **12**, 1–24.

23 S. G. Sepanlou, S. Safiri, C. Bisignano, K. S. Ikuta, S. Merat, M. Saberifiroozi, H. Poustchi, D. Tsoi, D. V. Colombara and A. Abdoli, *Lancet Gastroenterol. Hepatol.*, 2020, **5**, 245–266.

24 Deloitte_Access_Economics, *The economic cost and health burden of liver diseases in Australia*, 2013.

25 N. Shackel, K. Patel and J. McHutchison, in *Essentials of Genomic and Personalized Medicine*, Elsevier, 2010, pp. 645–660.

26 M. Koplay, M. Sivri, H. Erdogan and A. Nayman, *World J. Hepatol.*, 2015, **7**, 769.

27 R. Wiesner, E. Edwards, R. Freeman, A. Harper, R. Kim, P. Kamath, W. Kremers, J. Lake, T. Howard, R. M. Merion, R. R. Wolfe and R. Krom, *Gastroenterology*, 2003, **124**, 91–96.

28 J. Sumskiene, L. Kupcinskas, J. Pundzius and L. Sumskas, *Medicina*, 2005, **41**, 39–46.

29 G. D'Amico, G. Garcia Tsao and L. Pagliaro, *J. Hepatol.*, 2006, **44**, 217–231.

30 J. A. Lopez-Velazquez, N. C. Chavez-Tapia, G. Ponciano-Rodriguez, V. Sanchez-Valle, S. H. Caldwell, M. Uribe and N. Mendez-Sanchez, *Ann. Hepatol.*, 2014, **13**, 98–104.

31 H. J. Kim and H. W. Lee, *Clin. Mol. Hepatol.*, 2013, **19**, 105–115.

32 M. Lee, W. Kim, Y. Choi, S. Kim, D. Kim, S. J. Yu, J.-H. Lee, H. Y. Kim, Y. J. Jung, B. G. Kim, Y. J. Kim, J.-H. Yoon, K. L. Lee and H.-S. Lee, *PLoS One*, 2014, **9**, e100870.

33 S. Ullah, K. Rahman and M. Hedayati, *Iran. J. Public Health*, 2016, **45**, 558.

34 R. A. Gatti, *J. Pediatr.*, 1967, **70**, 117–119.

35 C. R. Trappes-Lomax, J. M. King and S. P. Paul, *J. Fam. Health Care*, 2013, **23**, 24–28.

36 M. J. Maisels, *Pediatr. Rev.*, 2006, **27**, 443–454.

37 C. Wells, A. Ahmed and A. Musser, *Mol. Cell. Neurosci.*, 2013, **38**, 377–382.

38 A. Ramachandran, *Paediatr. Child Health*, 2016, **26**, 162–168.

39 L. M. Gartner, C. T. Herrarias and R. H. Sebring, *Pediatrics*, 1998, **101**, 25–31.

40 R. Wong and B. Bhutani, *UpToDate*, 2020, vol. 21, **https://www.uptodate.com/contents/unconjugated-hyperbilirubinemia-in-the-newborn-interventions#:~:text=The%20three%20interventions%20used%20to,%2C%20photgherapy%2C%20and%20exchange%20transfusion.**

41 A. F. McDonagh, *J. Perinatol.*, 2001, **21**, S7–S12.

42 N. R. Finsen, *Br. Med. J.*, 1903, **1**, 1297.

43 A. Downes, *Proc. R. Soc. London*, 1877, **26**, 488–500.

44 R. J. Cremer, P. W. Perryman and D. H. Richards, *Lancet*, 1958, **271**, 1094–1097.

45 J. Lucey, M. Ferreiro and J. Hewitt, *Pediatrics*, 1968, **41**, 1047–1054.

46 R. H. Dobbs and R. Cremer, *Arch. Dis. Child.*, 1975, **50**, 833–836.

47 P. K. Vandborg, B. M. Hansen, G. Greisen and F. Ebbesen, *Pediatrics.*, 2012, **130**, e352–e357.

48 T.-C. Yu, C. Nguyen, N. Ruiz, S. Zhou, X. Zhang, E. A. Böing and H. Tan, *BMC Pediatr.*, 2019, **19**, 1–15.

49 T. W. R. Hansen, *Pediatr. Med.*, 2021, **5**, 1–14.

50 M. J. Maisels, *Pediatrics*, 2006, **118**, 805–807.

51 A. Beer, *Ann. Phys.*, 1852, **162**, 78–88.

52 I. Yamanouchi, Y. Yamauchi and I. Igarashi, *Pediatrics*, 1980, **65**, 195–202.

53 K. Grohmann, M. Roser, B. Rolinski, I. Kadow, C. Muller, A. Goerlach-Graw, M. Nauck and H. Kuster, *Pediatrics*, 2006, **117**, 1174–1183.

54 K. Vink, W. Schuurman and R. Van Gansewinkel, *Clin. Chem.*, 1986, **32**, 1389–1393.

55 Š. Hajzer, *J. Clin. Chem. Clin. Biochem.*, 1989, **27**, 445–449.

56 J. Vichapong, R. Burakham, N. Teshima, S. Srijaranai and T. Sakai, *Anal. Methods*, 2013, **5**, 2419–2426.

57 K. Amazon, F. Soloni and A. M. Rywlin, *Am. J. Clin. Pathol.*, 1981, **75**, 519–523.

58 S. C. Kazmierczak, A. F. Robertson, P. G. Catrou, K. P. Briley, B. L. Kreamer and G. R. Gourley, *Clin. Chem.*, 2002, **48**, 1096–1097.

59 J. G. Bell, M. P. Mousavi, M. K. Abd El-Rahman, E. K. Tan, S. Homer-Vanniasinkam and G. M. Whitesides, *Biosens. Bioelectron.*, 2019, **126**, 115–121.

60 W. Tan, L. Zhang, J. C. Doery and W. Shen, *Sens. Actuators, B*, 2020, **305**, 127448.

61 F. Shinya, *Tohoku J. Exp. Med.*, 1984, **143**, 249–251.

62 W. Spivak and W. Yuey, *Biochem. J.*, 1986, **234**, 101–109.

63 P. L. Jansen, H. T. Cuypers and W. H. Peters, *Eur. J. Clin. Invest.*, 1984, **14**, 295–300.

64 P. L. Jansen, W. H. Peters and A. R. Janssens, *J. Hepatol.*, 1986, **2**, 485–494.

65 M. Martelanc, L. Žiberna, S. Passamonti and M. Franko, *Talanta*, 2016, **154**, 92–98.

66 W. Spivak and M. C. Carey, *Biochem. J.*, 1985, **225**, 787–805.

67 G. Ma, J. Lin, W. Cai, B. Tan, X. Xiang, Y. Zhang and P. Zhang, *J. Pharm. Biomed. Anal.*, 2014, **92**, 149–159.

68 Y. S. Fung, D. X. Sun and C. Y. Yeung, *Electrophoresis*, 2000, **21**, 403–410.

69 C. Y. Yeung, Y. S. Fung and D. X. Sun, *Semin. Perinatol.*, 2001, **25**, 50–54.

70 Z. Nie and Y. S. Fung, *Electrophoresis*, 2008, **29**, 1924–1931.

71 H. Sun, Z. Nie and Y. S. Fung, *Electrophoresis*, 2010, **31**, 3061–3069.

72 T. Monteiro and M. G. Almeida, *Crit. Rev. Anal. Chem.*, 2019, **49**, 44–66.

73 L. Clark, *Trans. - Am. Soc. Artif. Intern. Organs*, 1956, **2**, 41–48.

74 L. C. Clark Jr and C. Lyons, *Ann. NY Acad. Sci.*, 1962, **102**, 29–45.

75 P. D'Orazio, *Clin. Chim. Acta*, 2003, **334**, 41–69.

76 E. B. Bahadır and M. K. Sezgintürk, *Anal. Biochem.*, 2015, **478**, 107–120.

77 F. Moussa, G. Kanoute, C. Herrenknecht, P. Levillain and F. Trivin, *Anal. Chem.*, 1988, **60**, 1179–1185.

78 J. Klemm, M. I. Prodromidis and M. I. Karayannis, *Electroanalysis*, 2000, **12**, 292–295.

79 M. A. Rahman, K.-S. Lee, D.-S. Park, M.-S. Won and Y.-B. Shim, *Biosens. Bioelectron.*, 2008, **23**, 857–864.

80 Q. Feng, Y. Du, C. Zhang, Z. Zheng, F. Hu, Z. Wang and C. Wang, *Sens. Actuators, B*, 2013, **185**, 337–344.

81 P. Kannan, H. Chen, V. T.-W. Lee and D.-H. Kim, *Talanta*, 2011, **86**, 400–407.

82 Z. Yang, X. Shang, C. Zhang and J. Zhu, *Sens. Actuators, B*, 2014, **201**, 167–172.

83 Z. Yang and C. Zhang, *Biosens. Bioelectron.*, 2011, **29**, 167–171.

84 X. Li and Z. Rosenzweig, *Anal. Chim. Acta*, 1997, **353**, 263–273.

85 W. Yang, J. Xia, G. Zhou, D. Jiang and Q. Li, *RSC Adv.*, 2018, **8**, 17854–17859.

86 Y. Andreu, M. Ostra, C. Ubide, J. Galbán, S. de Marcos and J. R. Castillo, *Talanta*, 2002, **57**, 343–353.

87 Y. Andreu, J. Galbán, S. de Marcos and J. R. Castillo, *Fresenius' J. Anal. Chem.*, 2000, **368**, 516–521.

88 A. K. Brown, J. Eisinger, W. E. Blumberg, J. Flores, G. Boyle and A. A. Lamola, *Pediatrics*, 1980, **65**, 767–776.

89 M. Santhosh, S. R. Chinnadayyala, A. Kakoti and P. Goswami, *Biosens. Bioelectron.*, 2014, **59**, 370–376.

90 H. S. Lee, M. M. Karim, S. M. Alam and S. H. Lee, *Luminescence*, 2007, **22**, 331–337.

91 N. Wu, W. J. Horvath and C. W. Huie, *Anal. Chim. Acta*, 1992, **269**, 99–107.

92 L. Palilis, A. Calokerinos and N. Grekas, *Anal. Chim. Acta*, 1996, **333**, 267–275.

93 L. P. Palilis, A. C. Calokerinos and N. Grekas, *Biomed. Chromatogr.*, 1997, **11**, 71–72.

94 C. Lu, J.-M. Lin and C. W. Huie, *Talanta*, 2004, **63**, 333–337.

95 C. Lu, G. Song, J.-M. Lin and C. W. Huie, *Anal. Chim. Acta*, 2007, **590**, 159–165.

96 P. Longhi, T. Mussini, S. Rondinini, G. Dada, P. Manitto and D. Monti, *Bioelectrochem. Bioenerg.*, 1987, **17**, 101–104.

97 B. Zeng, Z. Liu and X. Zhou, *Anal. Sci.*, 1994, **10**, 95–99.

98 B. Zeng and X. Zhou, *Fresenius' J. Anal. Chem.*, 1993, **347**, 382–387.

99 S. L. Jacques, I. S. Saidi, A. Ladner and D. Oelberg, *Proc. SPIE*, Laser-Tissue Interaction VIII, vol. 2975, 1997.

100 C. M. Wong, P. Van Dijk and I. Laing, *Arch. Dis. Child. Fetal Neonatal Ed.*, 2002, **87**, F137–F140.

101 C. C. Zabetta, I. Iskander, C. Greco, C. Bellarosa, S. Demarini, C. Tiribelli and R. Wennberg, *Neonatology*, 2013, **103**, 177–181.

102 M. Kamann, M. Henkel and T. Fischler, New jaundice meter for the tiniest of patients, *Press release*, Drägerwerk AG & Co. KGaA, 2013, p. 67e.

103 O. Starowicz, P. Edwards, P. Schmidt and P. Birch, *J. Paediatr. Child Health*, 2020, **56**, 283–288.

104 D. J. F. Pietrzyk and W. Clyde, in *Analytical chemistry*, Elsevier Inc., 1979, vol. 2, pp. 389–409.

105 T. Durduran, G. Yu, M. G. Burnett, J. A. Detre, J. H. Greenberg, J. Wang, C. Zhou and A. Yodh, *Opt. Lett.*, 2004, **29**, 1766–1768.

106 S. Kudavelly, P. Keswarpu and S. Balakrishnan, *2011 IEEE International Instrumentation and Measurement Technology Conference*, 2011, pp. 1–4.

107 C. C. Garber, *Clin. Chem.*, 1981, **27**, 1410–1416.

108 J. J. Cadusch, J. Meng, D. Wen, V. R. Shrestha and K. B. Crozier, *ACS Photonics*, 2022, **9**, 474–481.

109 O. Yossef Hay, M. Cohen, I. Nitzan, Y. Kasirer, S. Shahroor-karni, Y. Yitzhaky, S. Engelberg and M. Nitzan, *Sensors*, 2018, **18**, 3457.

110 W. Zijlstra, A. Buursma and W. Meeuwsen-Van der Roest, *Clin. Chem.*, 1991, **37**, 1633–1638.

111 J. Yadav, A. Rani, V. Singh and B. M. Murari, *Biomed. Signal Process. Control.*, 2015, **18**, 214–227.

112 M. Friebel, J. Helfmann, U. J. Netz and M. C. Meinke, *J. Biomed. Opt.*, 2009, **14**, 034001.

113 A. C. Ralston, R. K. Webb and W. B. Runciman, *Anaesthesia*, 1991, **46**, 202–206.

114 J. Farmer, in *Design of pulse oximeters*, ed. J. G. Webster, Taylor & Francis, 1997, pp. 34–52.

115 B. Chance, *Rev. Sci. Instrum.*, 1951, **22**, 634–638.

116 R. Rikmenspoel, *Appl. Opt.*, 1964, **3**, 351.

117 J. P. Ndabakuranye, A. E. Rajapaksa, G. Burchall, S. Li, S. Prawer and A. Ahnood, *IEEE Trans. Biomed. Eng.*, 2021, **69**, 983–990.

118 J. P. Ndabakuranye, J. Ryu, J. Kim, N. T. H. Le, J. Park and J. Kim, *J. Photochem. Photobiol., A*, 2019, **381**, 111869.

119 J. W. Severinghaus, History, status and future of pulse oximetry, *Continuous Transcutaneous Monitoring*, ed. A. Huch, R. Huch and G. Rooth, Springer, 1987, pp. 3–8.

120 J.-A. Collins, A. Rudenski, J. Gibson, L. Howard and R. J. B. O'Driscoll, 2015, vol. 11, pp. 194–201.

121 J. Liu, B. P.-Y. Yan, W.-X. Dai, X.-R. Ding, Y.-T. Zhang and N. Zhao, *Biomed. Opt. Express*, 2016, **7**, 4313–4326.

122 S. Shibata, *Angew. Chem., Int. Ed. Engl.*, 1976, **15**, 673–679.

123 J. Ennever, A. Costarino, R. Polin and W. Speck, *J. Clin. Invest.*, 1987, **79**, 1674–1678.

124 K. J. Laidler, *Chemical Kinetics*, Pearson Education Inc., 3rd edn, 1987.

125 H. B. Ahmad, S. Ahmad, M. A. Shad and M. Hussain, *Asian J. Chem.*, 2013, **25**, 7945–7948.

126 S. B. Dubin, S. Wardlaw and P. Jatlow, *Clin. Chim. Acta*, 1980, **101**, 193–207.

127 P. D. Berk, R. B. Howe, J. R. Bloomer and N. I. Berlin, *J. Clin. Invest.*, 1969, **48**, 2176–2190.

128 I. Goncharova, J. Jašprová, L. Vítek and M. Urbanová, *Anal. Biochem.*, 2015, **490**, 34–45.

129 A. M. Snell, *Ann. Intern. Med.*, 1935, **9**, 690–711.

130 S. Tungjitkusolmun, in *Design of Pulse Oximeters*, ed. J. G. Webster, Bristol: Institute of Physics, 1997, pp. 176–198.

131 S. J. Fearnley and J. M. Manners, *Anaesthesia*, 1993, **48**, 87–88.

132 B. O'driscoll, L. Howard and A. J. T. Davison, 2009, **63**, vi1-vi68.

133 D. Seidler, M. Hirschl and G. Roeggla, *Lancet*, 1993, **341**, 1600–1601.

134 K. Reynolds, J. Moyle, L. Gale, M. Sykes and C. Hahn, *Med. Biol. Eng. Comput.*, 1992, **30**, 629–635.

135 H. Kinoshita, N. Tanaka, A. Takakura, M. Jamal, A. Ito, M. Kumihashi, S. Kimura, K. Tsutsui, S. Matsubara and K. Ameno, in *Post Mortem Examination and Autopsy-Current Issues From Death to Laboratory Analysis*, IntechOpen, 2017.

136 K. Reynolds, J. De Kock, L. Tarassenko and J. Moyle, *Br. J. Anaesth.*, 1991, **67**, 638–643.

137 C.-K. Hsu, S.-Y. Tzeng, C.-C. Yang, J. Y.-Y. Lee, L. L.-H. Huang, W.-R. Chen, M. Hughes, Y.-W. Chen, Y.-K. Liao and S.-H. Tseng, *Biomed. Opt. Express*, 2015, **6**, 390–404.

138 S. G. Lichter, M. C. Escudié, A. D. Stacey, K. Ganesan, K. Fox, A. Ahnood, N. V. Apollo, D. C. Kua, A. Z. Lee and C. McGowan, *Biomaterials*, 2015, **53**, 464–474.

139 B. W. Bourgeois, in *Design of Pulse Oximeters*, CRC Press, 1997, pp. 69–83.

140 I. L. Azevedo, M. G. Morgan and F. Morgan, *Proc. IEEE*, 2009, **97**, 481–510.

141 M. Hamza and M. Hamza, *Proc. SPIE 2676, Biomedical Sensing, Imaging, and Tracking Technologies I*, 1996, **2676**, 341–350.

142 J. Piprek, *Appl. Phys. Lett.*, 2016, **109**, 021104.

143 P. J. Smalley, *Laser Ther.*, 2011, **20**, 95–106.

144 J. S. Schowalter, in *Design of Pulse Oximeters*, ed. J. G. Webster, CRC Press, 1997, pp. 84–98.

145 M. V. S. Reddy, in *Design of Pulse Oximeters*, CRC Press, 1997, pp. 99–109.

146 D. Chandrasekar, B. Arnetz, P. Levy and A. S. Basu, *Annu. Int. Conf. IEEE Eng. Med. Biol. Soc.*, 2012, 3243–3246.

147 Y. Mendelson, R. Duckworth and G. Comtois, *Conf. Proc. IEEE Eng. Med. Biol. Soc.*, 2006, 912–915.

148 S. Kästle, F. Noller, S. Falk, A. Bukta, E. Mayer and D. Miller, *Hewlett Packard J.*, 1997, **48**, 39–47.

149 H. García-Vázquez, F. C. Dualibe and G. Popov, *IEEE International Midwest Symposium on Circuits and Systems*, 2017, pp. 763–766.

150 N. Stuban and M. Niwayama, *Rev. Sci. Instrum.*, 2012, **83**, 104708.

151 T. Kugelstadt, in *Op amps for everyone*, Elsevier, 2nd edn, 2009, ch. 16, vol. 2, pp. 365–438.

152 M. R. Alam and S. Faruque, *IEEE Vehicular Networking Conference*, 2016, pp. 1–4.

153 P. T. Kwok and H. C. Luong, *IEEE Trans. Circuits Sys.*, 1999, **46**, 549–553.

154 Z. Feng, *Microchip Technology Inc.*, 2015, **DS00001525B**, 1–12.

155 A. Subero, in *Programming PIC Microcontrollers with XC8*, Springer, 1st edn, 2018, vol. 1, pp. 209–276.

156 D. Zhou and E. Greenbaum, *Implantable neural prostheses 1: Devices and applications*, Springer, 2009.

157 D. Zhou and E. Greenbaum, *Implantable neural prostheses 2: techniques and engineering approaches*, Springer Science & Business Media, 2010.

158 M. Rasouli and L. S. J. Phee, *Expert Rev. Med. Devices*, 2010, **7**, 693–709.

159 W.-S. Lee, J.-K. Lee, S.-A. Lee, J.-K. Kang and T.-S. Ko, *Surg. Neurol.*, 2000, **54**, 346–351.

160 A. Ahnood, K. E. Fox, N. V. Apollo, A. Lohrmann, D. J. Garrett, D. A. Nayagam, T. Karle, A. Stacey, K. M. Abberton, W. A. Morrison, A. Blakers and S. Prawer, *Biosens. Bioelectron.*, 2016, **77**, 589–597.

161 J. P. Ndabakuranye, H. Lee, I. Kayijuka, S. Baang and J. Park, *Sens. Mater.*, 2020, **32**, 2399–2408.

162 A. Ahnood, J. P. Ndabakuranye, S. Li, O. Kavehei and S. Prawer, *Eng. Res. Express*, 2020, **2**, 015036.

163 M. Wang, in *Engineering Materials For Biomedical Applications*, ed. T. S. Hin, World Scientific, 2004, vol. 1, pp. 8–29.

164 M. Saini, Y. Singh, P. Arora, V. Arora and K. Jain, *World J. Clin. Cases*, 2015, **3**, 52.

165 A. Ahnood, H. Meffin, D. J. Garrett, K. Fox, K. Ganesan, A. Stacey, N. V. Apollo, Y. T. Wong, S. G. Lichter and W. J. A. B. Kentler, *Adv. Biosyst.*, 2017, **1**, 1–10.

166 A. Ahnood, R. Cheriton, A. Bruneau, J. A. Belcourt, J. P. Ndabakuranye, W. Lemaire, R. Hilkes, R. Fontaine, J. P. Cook and K. Hinzer, *Adv. Biosyst.*, 2020, **4**, 2000055.

167 J. F. Mano, R. A. Sousa, L. F. Boesel, N. M. Neves and R. L. Reis, *Compos. Sci. Technol.*, 2004, **64**, 789–817.

168 H. Ghasemi, N. Thoppey, X. Huang, J. Loomis, X. Li, J. Tong, J. Wang and G. Chen, *iTherm*, 2014, **14**, 235–239.

169 A. M. Khorasani, M. Goldberg, E. H. Doeven and G. Littlefair, *J. Biomater. Tissue Eng.*, 2015, **5**, 593–619.

170 A. Kamal, M. Bashir, S. Firdous, T. Yasin, M. Tariq, M. Ikram, M. J. R. P. Mehmood and Chemistry, *Radiat. Phys. Chem.*, 2016, **118**, 102–106.

171 K. R. Kesler, W. S. Dabbs and D. A. Holmes, Implementation of Biomaterials for the Encapsulation of Sensors, *Chancellor's Honors Program Projects*, University of Tennessee, Knoxville, 2006, **https://trace.tennessee.edu/utk_chanhonoproj/980**.

172 C. Ding, P. Bogorzi, M. Sigurdson, C. Meinhart and N. MacDonald, in *A Solid-state Sensors, Actuators Microsystems Work*, Hilton Head Island, SC, 2010, pp. 1–4, DOI: **10.31438/trf.hh2010.100**.

173 X. Zhang, J. P. Ndabakuranye, D. W. Kim, J. S. Choi and J. Park, *Electron. Mater. Lett.*, 2015, **11**, 964–972.

174 J. P. Ndabakuranye, S. Prawer and A. Ahnood, *Engineering Proceedings (ecsa-8)*, 2021, vol. 10, pp. 74–77.

175 J. P. Ndabakuranye, S. Prawer and A. Ahnood, *IEEE Xplore (HI-POCT)*, 2022, vol. 7, pp. 95–98.

176 J. Min, J. R. Sempionatto, H. Teymourian, J. Wang and W. Gao, *Biosens. Bioelectron.*, 2021, **172**, 112750.

177 B. Kaur, S. Kumar and B. K. Kaushik, *Biosens. Bioelectron.*, 2022, **197**, 113805.

178 G. Zhu, Y. Wang, Z. Wang, R. Singh, C. Marques, Q. Wu, B. K. Kaushik, R. Jha, B. Zhang and S. Kumar, *IEEE Trans. Instrum. Meas.*, 2021, **71**, 1–9.

179 S. Kumar, Z. Guo, R. Singh, Q. Wang, B. Zhang, S. Cheng, F.-Z. Liu, C. Marques, B. K. Kaushik and R. Jha, *J. Lightwave Technol.*, 2021, **39**, 4069–4081.

180 B. Kaur, S. Kumar and B. K. Kaushik, *IEEE Sens. J.*, 2021, **21**, 23957–23964.

181 R. Singh, S. Kumar, F.-Z. Liu, C. Shuang, B. Zhang, R. Jha and B. K. Kaushik, *Biosens. Bioelectron.*, 2020, **168**, 112557.